ORIGINAL ARTICLE

Connectivity of the Cingulate Sulcus Visual Area (CSv) in Macaque Monkeys

V De Castro [1,2], AT Smith[3], AL Beer[4], C Leguen[1,2], N Vayssière[1,2], Y Héjja-Brichard [1,2], P Audurier[1,2], BR Cottereau[1,2] and JB Durand[1,2]

[1]Université de Toulouse, Centre de Recherche Cerveau et Cognition, Toulouse, France, [2]Centre National de la Recherche Scientifique, Toulouse Cedex, France, [3]Department of Psychology, Royal Holloway, University of London, Egham TW20 0EX, UK and [4]Institut für Psychologie, Universität Regensburg, 93053 Regensburg, Germany

Address correspondence to Vanessa De Castro, CNRS CERCO UMR 5549, Pavillon Baudot CHU Purpan / BP 25202, 31052 Toulouse Cedex 03, France. Email: vanessa.decastro@cnrs.fr; Jean-Baptiste Durand, CNRS CERCO UMR 5549, Pavillon Baudot CHU Purpan / BP 25202, 31052 Toulouse Cedex 03, France. Email: jbdurand@cnrs.fr.

Abstract

In humans, the posterior cingulate cortex contains an area sensitive to visual cues to self-motion. This cingulate sulcus visual area (CSv) is structurally and functionally connected with several (multi)sensory and (pre)motor areas recruited during locomotion. In nonhuman primates, electrophysiology has shown that the cingulate cortex is also related to spatial navigation. Recently, functional MRI in macaque monkeys identified a cingulate area with similar visual properties to human CSv. In order to bridge the gap between human and nonhuman primate research, we examined the structural and functional connectivity of putative CSv in three macaque monkeys adopting the same approach as in humans based on diffusion MRI and resting-state functional MRI. The results showed that putative monkey CSv connects with several visuo-vestibular areas (*e.g.,* VIP/FEFsem/VPS/MSTd) as well as somatosensory cortex (*e.g.,* dorsal aspects of areas 3/1/2), all known to process sensory signals that can be triggered by self-motion. Additionally, strong connections are observed with (pre)motor areas located in the dorsal prefrontal cortex (*e.g.,* F3/F2/F1) and within the anterior cingulate cortex (*e.g.,* area 24). This connectivity pattern is strikingly reminiscent of that described for human CSv, suggesting that the sensorimotor control of locomotion relies on similar organizational principles in human and nonhuman primates.

Key words: connectivity, locomotion, MRI, primates, sensorimotor

Introduction

Primates are endowed with a very wide range of locomotor behaviors (Stern and Oxnard 1973), and they rely on several sources of sensory feedback to adjust body posture, gait, and heading direction during locomotion (Takakusaki 2017). For instance, somatosensory signals indicate the kinematics of the body parts recruited during self-motion, while the acceleration and swaying of the body that they produce are monitored as head movements by the vestibular system. Another sensory consequence of self-motion is optic flow (Gibson 1950), that

is, the continuous retinal image change caused by relative motion between the eyes and the visual surroundings. The visual modality playing a central role in primates, optic flow is considered a major signal for the control of locomotion (Warren et al. 2001). However, the way this sensorimotor process is actually implemented in the brain is only partially understood (Sherrill et al. 2015). Another open issue is whether the control of locomotion is implemented similarly in human and nonhuman primates. By forsaking arboreal locomotion and becoming bipedal walkers, humans have developed unique anatomical

adaptations such as the dual curvature of the vertebral column or the disappearance of an opposable hallux (see Schmidt 2011 for review). This uniqueness might well extend to the brain structures supporting the control of locomotion.

In recent years, neuroimaging studies have identified a potential candidate for the online control of locomotion in the human brain. A small region of the posterior cingulate cortex was first documented with regard to its sensitivity to visual cues to self-motion (Antal et al. 2008; Wall and Smith 2008; Fischer et al. 2012). Although optic flow stimuli evoke responses in a large and distributed set of human brain areas, such as the dorsal medial-superior temporal (MSTd) and ventral intraparietal (hVIP) areas, this cingulate sulcus visual (CSv) area was unique in remaining largely silent when the optic flow was made inconsistent with locomotion (see Smith et al. 2017 for review). Interestingly, CSv was later shown to respond also to vestibular cues to self-motion (Smith et al. 2012). Both the multisensory properties of CSv and the fact that it is located in a portion of the brain involved in spatial sensorimotor processes (Vogt et al. 1992; Kravitz et al. 2011) suggested a potential involvement in the control of locomotion. Recently, Smith and collaborators (2018) have brought strong support to this hypothesis by characterizing the structural and functional connectivity of CSv through both diffusion-weighted magnetic resonance imaging (DWI) and resting-state functional MRI (rs-fMRI). Besides confirming the connectivity of CSv with areas processing visual and/or vestibular cues to self-motion, they could also document connections with the somatosensory cortex. Importantly, CSv was also shown to connect with (pre)motor areas located in the anterior cingulate and prefrontal cortices (Smith et al. 2018), suggesting that it might be involved in the multisensory control of locomotion. In agreement with this finding, CSv has recently been shown to respond to active leg movements (Serra et al. 2019).

In macaque monkeys, electrophysiological studies have identified neurons integrating visual and vestibular cues to self-motion in several areas such as MSTd (Duffy 1998), VIP (Colby et al. 1993; Bremmer et al. 2002; Schlack et al. 2002; Chen et al. 2011a), a portion of the frontal eye field (FEFsem) involved in smooth eye movements (Gu et al. 2016) and the visual posterior sylvian (VPS) area (Guldin and Grüsser 1998; Chen et al. 2011b). For most of these areas, functional equivalents were later identified in the human brain (see Smith et al. 2017 for review). This is notably the case for hMSTd (Dukelow et al. 2001) and hVIP (Bremmer et al. 2001). By contrast, when CSv was first identified in the human brain, no functional equivalent had been previously documented in macaques. This was recently achieved by an fMRI study (Cottereau et al. 2017) that adopted the protocol used to identify CSv in humans, in which brain responses evoked by optic flow stimuli that were either consistent or inconsistent with self-motion were contrasted (Wall and Smith 2008). With such a design, a small area responding almost exclusively to visual cues consistent with self-motion was observed in the posterior cingulate cortex of macaque monkeys. Currently, we do not know whether this putative monkey CSv (pmCSv) responds to vestibular cues to self-motion, nor whether it connects to both (multi)sensory and (pre)motor areas as does human CSv (Smith et al. 2018).

The present study addresses these issues, with the aim of assessing the degree of similarity between the connectivity pattern of human CSv and that of its putative counterpart in monkey. To that end, we have implemented a connectivity study similar to that performed in humans (Smith et al. 2018) with the 3 macaque monkeys in which pmCSv had been functionally identified previously (Cottereau et al. 2017). By combining diffusion-MRI (structural connectivity) and rs-fMRI (functional connectivity), we show that pmCSv connects with a set of visual and/or vestibular areas, with the dorsal portion of somatosensory areas and also with (pre)motor areas of the anterior cingulate and prefrontal cortices. Overall, the connectivity pattern we document for pmCSv is strikingly similar to that previously described for human CSv with a similar approach. These results indicate that despite of their distinct locomotor adaptations, human and non-human primates might rely on a highly preserved cortical organization for the online control of locomotion.

Material and Methods

Animals

Three female rhesus macaques: M01, M02, and M03 (age: 15–17 years; weight: 5–8 kg) participated in this experiment. Animal housing, handling, and all experimental protocols (surgery and MRI recordings) followed the guidelines of the European Union legislation (2010/63/UE) and of the French Ministry of Agriculture (décret 2013–118). The project was approved by a local ethics committee (CNREEA code: C2EA—14) and received authorization from the French Ministry of Research (MP/03/34/10/09). The 3 animals were housed together in a large, enriched enclosure and could thus develop social and foraging behaviors. They returned to their individual cages to be fed twice a day, with standard primate biscuits supplemented with various types of fruits and vegetables. Health inspections were carried out quarterly on these animals. Details about the animals' surgical preparation are provided in Cottereau et al. (2017).

Localization of pmCSv and Other Self-Motion-Sensitive Visual Areas

These 3 animals are the same as those previously involved in the functional MRI study (Cottereau et al. 2017) that allowed identification of the cortical regions sensitive to visual cues to self-motion by contrasting the blood-oxygenation-level-dependent (BOLD) responses evoked by optic flow stimuli that were consistent or inconsistent with self-motion (Wall and Smith 2008). With this approach, we could localize the putative monkey CSv (pmCSv) in all 3 animals (4/6 hemispheres). We also documented other cortical areas processing visual cues to self-motion: the dorsal medial-superior temporal (MSTd) area (6 hemispheres), the medial superior temporal polysensory (STPm) area (5 hemispheres), the ventral intraparietal (VIP) area (6 hemispheres), 7a/Opt (5 hemispheres), the visual posterior sylvian (VPS) area (5 hemispheres) and the portions of the frontal eye field devoted to smooth eye movements (FEFsem; 5 hemispheres) and to saccades (FEFsac; 4 hemispheres). The MNI coordinates of these areas are available in Table 1 of Cottereau et al. (2017).

Scanning

Prior to the scanning sessions, the animals were installed in a sphinx position within an MRI-compatible primate chair, their head restrained by the surgically implanted head-post. Whole-brain images were acquired on a 3 Tesla clinical MR scanner (Phillips Achieva) using a custom 8-channel phased array coil

Table 1 List of template-based areas showing significant structural and functional connectivity with pmCSv, with their MNI coordinates on the right hemisphere of monkey F99, their structural and functional t-values relative to V1/V2/V3, their normalized strength of connectivity, the numbers of ipsilateral and contralateral hemispheres above the V1/V2/V3 structural and functional baselines and their main function(s)

Area	Center of mass XYZ (mm) – MNI			Structural t-value	Functional t-value	Connectivity strength (%)	Nb hemi. (ipsi / contra)	Function(s)
23 (pmCSv)	4.8	6.2	5.6	31.7	6.3	10.4	6/6	Premotor & visuo-vestibular
F3	4.6	23.3	14.7	23.6	6.4	8.6	6 / 6	Premotor
1	12.7	7.1	14.3	9.9	10.5	7.5	6 / 6	Somatosensory
24d	5.1	23.4	9.8	17.6	5.7	6.9	6 / 6	Premotor
3	16.0	11.3	10.7	12.7	7.9	6.9	6/6	Somatosensory
F1	13.1	14.5	14.5	14.5	6.6	6.6	6 / 6	Motor
7 m/PGm	5.0	-0.5	11.2	11.1	5.7	5.4	6/6	Visuo-vestibular
F2	11.0	22.4	15.9	11.7	5.1	5.2	6/6	Premotor
7op (VPS)	21.9	4.0	5.3	7.8	6.4	5.0	6/6	Visuo-vestibular
F4	20.4	19.6	10.5	13.4	3.3	4.7	5 / 5	Premotor
8 m (FEFsem)	15.6	24.7	10.4	12.6	3.5	4.6	5 / 6	Visuo-vestibular
VIP	12.0	0.1	8.8	11.5	3.7	4.5	5 / 4	Visuo-vestibular
F6	4.9	31.3	11.8	8.5	3.2	3.6	6 / 5	Premotor
Tpt	22.1	-1.0	9.2	6.4	3.5	3.2	5 / 5	Visuo-vestibular
MST	18.5	-4.2	8.3	5.2	4.0	3.2	5 / 6	Visuo-vestibular
LIP	14.1	-1.9	12.2	4.7	4.1	3.1	5 / 5	Visuo-vestibular
2	21.6	8.8	9.2	4.3	3.9	3.0	4 / 4	Somatosensory
MT	20.2	-6.1	5.3	3.6	4.2	2.9	4 / 5	Visual
STPc	26.1	-1.4	6.3	2.9	3.4	2.4	4 / 4	Visuo-somatosensory
V6	6.0	-12.4	3.5	4.2	2.7	2.3	5 / 4	Visual

Areas are listed in decreasing order of connectivity strength.

(RapidBiomed) specially designed to fit the skull of our animals. Details about the functional MRI study that localized the regions sensitive to visual cues to self-motion in our 3 animals are provided in Cottereau et al. (2017). Below, we only describe the 5 scanning sessions that each of them underwent under light anesthesia for (1) creating brain and cortical surface templates (1 session), (2) assessing the structural connectivity through diffusion MRI (1 session) and (3) estimating the functional connectivity with resting-state functional MRI (3 sessions). The light anesthesia administered to our animals is unlikely to have a detrimental impact on the functional connectivity we measured from resting state fMRI. It has been shown that functional connectivity can be measured reliably in macaques even with ketamine-induced anesthesia causing profound loss of consciousness (Vincent et al. 2007). Moreover, by silencing cognitive processes, the anesthesia is expected to provide functional connectivity patterns matching more closely the structural ones (Barttfeld et al. 2015).

Brain and Cortical Surface Templates

Data Acquisition
Anatomical and functional brain templates were built from acquisitions made in a single session on lightly anesthetized animals (Zoletil 100:10 mg/kg and Medetomidine: 0.04 mg/kg). The animals' constants were monitored during the whole session (about 1 hour) with an MR compatible oximeter. During that session, we acquired four T1-weighted anatomical volumes by a magnetization-prepared rapid-acquisition gradient-echo sequence (MPRAGE; repetition time [TR]: 10.3 ms; echo time [TE]: 4.6 ms; flip angle: 8°; voxel size: $0.5 \times 0.5 \times 0.5$ mm; 192 sagittal slices with no inter-slice gap; field of view [FOV]: 160 $\times$ 160 mm), and 300 T2∗-weighted functional volumes by a gradient-echo sequence with echo-planar read-out (GE-EPI; TR: 2000 ms; TE: 30 ms; flip angle: 90°; SENSE factor: 1.6; voxel size: $1.25 \times 1.25 \times 1.5$ mm; 32 axial slices with no inter-slice gap; FOV:

100×100 mm). These T1 and EPI volumes were used to construct individual structural and functional templates, respectively.

Templates and Cortical Surfaces
The anatomical template was obtained by realigning and averaging the four T1-weighted volumes. It was then aligned to the MNI space of the 112RM-SL template (McLaren et al. 2009, 2010). Cortical surface reconstructions were performed using the CARET software (Van Essen et al. 2001). The functional template was obtained by realigning and averaging the 300 functional volumes. Affine and non-rigid normalization parameters bringing the functional template onto the anatomical template were estimated from the gray matter maps of both templates, using the normalization tools of the SPM12 software.

Cortical Surface Registration
For surface-based group analyses, each of the 6 individual cortical surfaces (left and right hemispheres of the 3 monkeys) was non-rigidly registered to the right cortical surface of the reference monkey F99 available in the CARET software (Van Essen 2002). For this, individual left cortical surfaces were first flipped left–right. All surfaces were then submitted to a non-rigid variant of the iterative closest point algorithm (Amberg et al. 2007) implemented in Matlab (https://www.github.com/charlienash/nricp). Results of this non-rigid registration are shown in Supplementary Figure 1.

Structural Connectivity (Diffusion MRI)

Data Acquisition
Each animal underwent one session of diffusion-weighted MRI recordings under light anesthesia (Medetomidine: 10 µg/kg, Ketamine: 10 mg/kg). Data was acquired in each subject by a spin-echo sequence with echo-planar read-out (TR: 7132 ms; TE: 62 ms; flip angle: 90°; voxel size: $1 \times 1 \times 1$ mm; 32 axial slices with no inter-slice gap; FOV: 120 $\times$ 120 mm, EPI factor: 55). We

had to slightly increase the number of axial slices (34) and the TR (7578 ms) for monkey M03. The DWI sequence contained a first volume without diffusion weighting ($b = 0$ s/mm^2) followed by diffusion-weighted images isotropically distributed along 128 directions with a b-value of 1000 s/mm^2. At the end of the sequence, an additional volume without diffusion weighting was acquired, but with an inverted polarity of phase encoding (inverted b-zero) in order to estimate and correct the susceptibility-induced off-resonance field. This sequence was repeated three times in order to increase the signal-to-noise ratio. The total imaging time was about 45 minutes.

Preprocessing
DICOM images were converted to NIFTI format using dcm2niigui (distributed by MRIcron), and then processed with the FMRIB software library (FSL, version 6.0.1) (Jenkinson et al. 2012). First, we applied an intra-modal motion correction to finely align the 128 volumes (one per direction) of the DWI sequence, and an intermodal affine registration to the inverted b-zero volume (Jenkinson et al. 2002). Then, images were reoriented and labels corrected (because of the monkeys' sphinx position within the bore of the scanner) using FSL tools. Second, the analysis of DWI was performed by the Diffusion Toolbox (FDT, version 5.0) (Behrens et al. 2007). This included corrections for susceptibility-induced off-resonance field (Andersson et al. 2003) and eddy current distortions (Andersson and Sotiropoulos 2016). Distributions of diffusion parameters at each voxel were estimated by means of Markov Chain Monte Carlo sampling. This modeling approach detects white matter regions of complex fiber architecture and uses automatic relevance detection to prevent the modeling of multiple fibers when inappropriate. Moreover, we made the registration within FDT to obtain the transformation matrices between diffusion and structural space.

Whole-Brain Structural Connectivity of pmCSv
Probabilistic tractography was performed with the FDT toolbox (Behrens et al. 2007) in individual diffusion space as in previous studies (Beer et al. 2011; Smith et al. 2018). All trajectories were seeded from each voxel included in the whole brain mask. We examined the probability of streamlines passing through pmCSv (waypoint mask). For each voxel of the seed mask, 5000 streamlines were sampled (maximum steps: 2000, step length: 0.5 mm, curvature threshold: 0.2). A loop-check for preventing circular pathways was applied. Linear registrations (see above section "Preprocessing") were applied for transforming tracking results into structural space. As in our previous work (Smith et al. 2018), the accumulated numbers of streamlines, or track frequencies (*f-track*), were converted into track probabilities (*p-track*) by dividing the log-scaled track frequency by the maximum log-scaled track frequency. Then, track probabilities were thresholded (*p-track* > 0.5). Equivalent thresholds were used in the previous studies (Behrens et al. 2003). Afterwards, track probabilities in volumetric space at the gray matter/white matter border were projected onto the individual cortical surfaces as follows: for all the surfaces' nodes, track probabilities were obtained by trilinear interpolation from 7 sampling points along the nodes' normal vectors (from −1 to +1 mm), to account for cortical thickness (1.5–2.5 mm in macaques). For each node, the higher track probability value was retained. Individual surface maps of structural connectivity were further grouped into 6 ipsilateral ones (left and right cortical surfaces for left and right pmCSv, respectively) and 6 contralateral ones (left and right cortical

surfaces for right and left pmCSv, respectively). Group results were obtained by projecting the ipsilateral and contralateral structural connectivity maps onto the right cortical surface of the reference monkey F99. At the group level, ipsilateral or contralateral track terminations (structural connectivity with pmCSv) were considered relevant if they exceeded the track probability threshold (*p-track* > 0.5) in at least half (3/6) of the hemispheres, as in previous studies (Beer et al. 2011).

ROI-Based Structural Connectivity of pmCSv
The volumetric masks of each region of interest (ROI), pmCSv, FEFsem, FEFsac, VPS, VIP, 7a, MSTd and STPm, were defined individually, based on the MNI coordinates given by Cottereau et al. (2017). Using FSL tools, we created a mask for each of these ROIs. More specifically, these masks corresponded to spheres of 1.5 mm radius, centered on the ROI's local maxima, before being binarized. Finally, these ROI masks were transformed to diffusion space for subsequent analysis performed by the FDT. The tracking algorithm was seeded in the voxels of pmCSv. Here, the mean track probabilities of the specific target ROIs were analyzed.

Functional Connectivity (Resting-State Functional MRI)

Data Acquisition
Each animal underwent three sessions of rs-fMRI recordings under slight anesthesia (Medetomidine: 10 μg/kg, Ketamine: 10 mg/kg). Each session lasted less than 1 hour, during which two runs of 25 minutes (600 volumes per run) were recorded. Data were acquired by gradient echo-planar imaging (GE-EPI; TR: 2000 ms; TE: 30 ms; flip angle: 90°; SENSE factor: 2; voxel size: $1.25 \times 1.25 \times 1.8$ mm; 25 axial slices with no inter-slice gap; FOV: 100 x 100 mm).

Preprocessing
The first 5 volumes of each run were discarded. The remaining functional images were first slice-time corrected to compensate for the delay caused by the sequential (interleaved) acquisition of the slices. A mean image was then generated for each run for co-registration with the individual functional template. Co-registration parameters were then combined with the normalization parameters transforming the individual functional template to the individual anatomical template. Those combined parameters were then applied to all the functional images of the run in a single interpolation step, which was also used to resample the functional volumes to $1 \times 1 \times 1$ mm voxels. No smoothing was applied to the volumetric data. After checking the absence of temperature-induced drifts during the acquisition of the functional volumes, rigid realignment was also omitted since the animals were anesthetized with their head immobilized by the head post. To regress out the signal fluctuations caused by physiological and/or environmental noise, time courses of voxels outside the brain (muscles, eyes, etc.) were extracted and 10% of the voxels with the highest temporal variance were submitted to a principal component analysis (PCA) after z-score normalization (Héjja-Brichard et al. 2020). The 12 first PCA components were used to regress out all signal fluctuations correlating with those noise regressors within the brain voxels. Functional data were then projected from volumetric space to surface space by trilinear interpolation along the surface nodes (7 sampling points per node along their normal vector; from −0.75 to +0.75 mm). The 7 functional time courses were first converted to percent signal change and then averaged

in a single mean time course attributed to the surface's node. Finally, both surface-based spatial smoothing (Gaussian kernel; FWHM = 2 mm) and temporal band-pass filtering were applied to the functional data. The RESTplus V1.23 toolbox (Jia et al. 2019) was used for temporal filtering in the range [0.01—0.1 Hz].

Whole-Brain Functional Connectivity of pmCSv
We first averaged the time courses from the surface nodes belonging to a given pmCSv ROI to constitute a seed time course. We then computed the (partial) correlation coefficients (r-values) between this seed time course and the time courses attached to all the nodes of both left and right cortical surfaces. This was done separately for each of the 6 runs collected per monkey. Correlation coefficients were first normalized by a Fisher Z-transformation and then averaged across the 6 runs for producing individual whole-brain maps of resting-state functional connectivity for pmCSv. For intersubject normalization and statistical analyses, these individual maps were shown as z-value maps (by subtracting from each correlation value the whole-brain mean and dividing it by the whole-brain standard deviation). We used a mean z-value of 1.96 (P value < 0.05) as a statistical threshold for the individual functional connectivity maps. Individual maps of functional connectivity were further grouped into 6 ipsilateral ones (left and right cortical surfaces for left and right pmCSv, respectively) and 6 contralateral ones (left and right cortical surfaces for right and left pmCSv, respectively). Group results were obtained by projecting the ipsilateral and contralateral functional connectivity maps onto the right cortical surface of the reference monkey F99. Ipsilateral or contralateral connectivity with pmCSv was considered relevant at the group level, if it was above our individual statistical threshold (z-value > 1.96) in at least half (3/6) of the hemispheres (as in Cottereau et al. 2017). Although cortical sites with significant negative correlations (z-value < −1.96) were sometimes observed in individual correlation maps (Supplementary Fig. 2), none was confirmed at the group level (i.e., in at least half of the hemispheres). For that reason, only positive correlations are considered here.

ROI-Based Functional Connectivity of pmCSv
The ROIs defined in individual structural volumetric space for FEFsem, FEFsac, VPS, VIP, 7a, MSTd and STPm were first projected onto the corresponding individual cortical surfaces. For each ROI, we determined the surface node corresponding to the center of mass of the projection and all the nodes less than 1 mm away were retained. Functional time courses from all these nodes were then averaged to produce the time course of that ROI, and the average was finally correlated to that of pmCSv (defined in the same way). For each ROI, the operation was repeated run per run and the correlation coefficients were finally averaged across runs after normalization with the Fisher Z-transformation.

Atlas-Based Analysis of Structural and Functional Connectivity

We performed an atlas-based analysis of the strength of both structural and functional connectivity across the 91 areas of the M132 atlas (Markov et al. 2014) registered onto the right cortical surface of monkey F99. Since structural connectivity measures (track probabilities) may have a nonzero value even by chance, the connectivity strength was evaluated relative to a reference baseline. For interspecies comparison purposes, we followed the approach used by Smith et al. (2018) and used as baseline the

average strength of connectivity across 3 areas, which are not thought to share direct cortico-cortical connection with pmCSv, that is, the first, second, and third visual areas (V1/V2/V3). Note that these areas and pmCSv might nevertheless hold indirect connections, since they all belong to the network of visually responsive areas. Hence, we favored a conservative criterion for evaluating the structural connectivity of pmCSv. Although the functional connectivity measures (partial correlation coefficients) do not have the same baseline limitation, we adopted the same strategy so that functional connectivity could also be evaluated with respect to the V1/V2/V3 baseline. For each area of the atlas, the mean structural connectivity (*i.e.*, mean p-track) and mean functional connectivity (*i.e.*, mean Fisher Z-transformed r-value) with pmCSv were computed for each of the 6 ipsilateral and 6 contralateral hemispheres. Based on the high similarity between the ipsilateral and contralateral connectivity strengths, they were grouped for subsequent statistical analyses. Finally, we compared the strength of pmCSv connectivity of each target area (M132 atlas) with the baseline connectivity strength (based on V1/V2/V3) by one-sample t-tests (two-tailed). An area was considered to be statistically more connected to pmCSv than areas V1/V2/V3 if its t-value > 2.6 (P value < 0.05) in both structural and functional domains. For these areas, we derived a normalized measured of combined connectivity with the following formula:

$$Connectivity\ Strength\ (\%) = \left(0.5 \times \frac{t_{structural}}{\sum t_{structural}} + 0.5 \times \frac{t_{functional}}{\sum t_{functional}} \right) \times 100 \quad (1)$$

where the t-values measured in the structural and functional domains for a given area ($t_{structural}$ and $t_{functional}$) are averaged after normalizing by the sum of the t-values across all areas showing significant deviation from the V1/V2/V3 reference ($\Sigma t_{structural}$ and $\Sigma t_{functional}$). This approach allows weighting structural and functional connectivity equally regardless of their respective overall sensitivity.

Results

Localization of the Putative Monkey CSv

The putative monkey counterpart of human CSv had been previously localized in each of the 3 monkeys involved in the present study based on the contrast between the brain responses to consistent and inconsistent optic flow stimuli (Cottereau et al. 2017) and replicating the design used to localize CSv in humans (Wall and Smith 2008). The individual statistical parametric maps are shown in Figure 1A, projected on inflated representations of the animals' left and right cortical surfaces. Notably, significant activations (t-value > 3.1; P value < 0.001 uncorrected) are found within the posterior cingulate sulcus in both hemispheres of M02 and in the left hemispheres of M01 and M03 (black circles; symmetrical locations within the right hemispheres of M01 and M03 are also indicated with dotted black circles).

When the statistical parametric maps from the 6 hemispheres are projected onto the right cortical surface of monkey F99 (see Methods section), these cingulate activations partially overlap across 4 of the 6 hemispheres (Fig. 1B), defining a restricted region that we defined as the putative monkey CSv (pmCSv). Figure 1C shows the mean t-value map for all the regions in which significant activations were observed in at least 3 out of the 6 hemispheres, together with the local statistical maxima (MSTd, STPm, VIP, VPS, 7a, FEFsem, FEFsac) documented in our previous study (Cottereau et al. 2017). Note that this new surface-based analysis reveals a supplementary local maximum within the dorsal-most part of the lunate sulcus, lying in
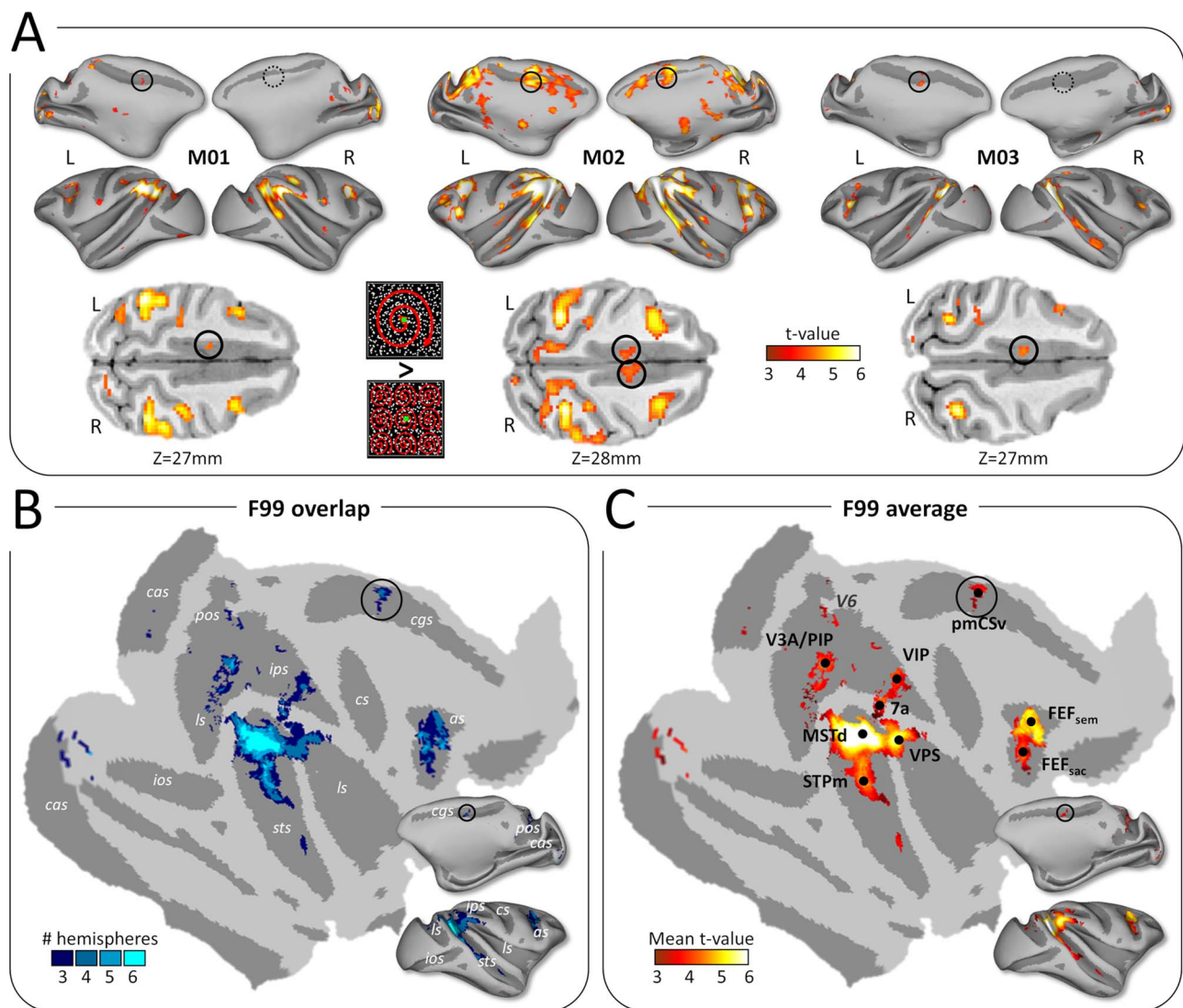
Figure 1. Cortical activations for egomotion-consistent optic flow stimuli. (A) Illustration of the egomotion-consistent (EC) and inconsistent (EI) optic flow stimuli and t-value maps for the contrast EC > EI in monkeys M01, M02 and M03 (from Cottereau et al. 2017). Significant activations (t-value > 3.1, P < 0.001 uncorrected) are color-coded in red to white and projected onto medial and lateral views of the inflated left and right cortical surfaces of the individual monkeys. Putative monkey CSv (pmCSv) was found in 4/6 hemispheres (black circles) and the corresponding location is indicated in the other 2 hemispheres (dotted black circles). Activations of pmCSv in the left hemisphere of M01, M02, and M3 and in the right hemisphere of M02 are also shown on horizontal slices through the native volumetric space (black circles in the lower row of the panel). (B) Overlap of the activation maps across the 6 individual cortical surfaces. Individual maps were registered and projected onto flattened and inflated representations of the right cortical hemisphere of monkey F99 (see Methods section). Only activation sites found in at least 3/6 hemispheres are shown (cas: calcarine sulcus; pos: parieto-occipital sulcus; cis: cingulate sulcus; ips: intraparietal sulcus; ls: lateral sulcus; ios: inferior occipital sulcus; sts: superior temporal sulcus; cs: central sulcus; as: arcuate sulcus). (C) Average activations (mean t-value) across the sites that were significant in at least 3/6 hemispheres. Black dots indicate the local maxima of this group analysis (V3A/PIP, MSTd, STPm, VIP, 7a, FEFsem, FEFsac and pmCSv). See Supplementary Figure 4A for area V6 (marked with dark gray).

between the medial border of area V3A and the latero-posterior border of the posterior intraparietal (PIP) area according to the atlas of Markov et al. (2014). The detection of this additional activation focus is probably due to the improved procedure for interindividual cortical surface registration used in the present study (see Supplementary Fig. 1).

Whole-Brain Structural Connectivity of pmCSv Based on Diffusion MRI

First, we used the diffusion MRI data to create individual whole-brain probabilistic maps of structural connectivity with left and right pmCSv (Figure 2A and B, respectively). These maps are shown on medial and lateral views of the inflated left and right cortical surfaces of the various monkeys M01, M02, and M03. In all 3 animals, structural connectivity (p-track > 0.5) was observed within a widespread network encompassing the temporal, parietal and frontal lobes, and including a large portion of the cingulate cortex. Remarkably, the cortical distribution of significant structural connectivity is very similar between (1) left and right pmCSv, (2) ipsilateral and contralateral hemispheres, and (3) the 3 monkeys.

The strong interindividual and interhemispheric similarity is well illustrated when projecting all the individual structural
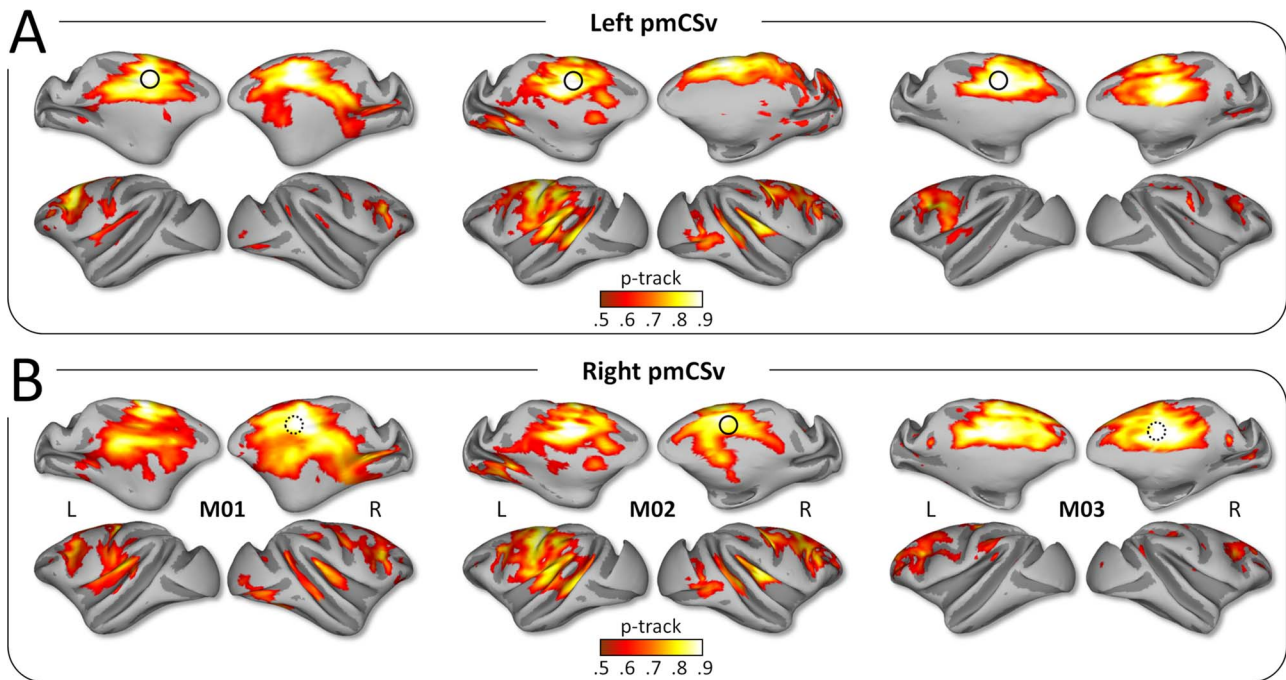
Figure 2. Structural connectivity: individual results. Whole-brain structural connectivity (diffusion MRI) of the left pmCSv (*A*) and the right pmCSv (*B*). Individual track probabilities (*p*-track) maps are projected onto medial and lateral views of the inflated left and right cortical surfaces for the 3 monkeys (threshold: *p*-track > 0.5).

connectivity maps onto flattened and inflated representations of the right cortical surface of the reference monkey F99. By focusing on the cortical regions exhibiting supra-threshold connectivity in at least half (3/6) of the individual hemispheres, we could confirm that in both ipsilateral (Fig. 3A) and contralateral (Fig. 3B) hemispheres, pmCSv was connected with a large number of cortical areas notably encompassing the cingulate (cis), arcuate (as), central (cs), intraparietal (ips), lateral (ls) and superior temporal (sts) sulci (see Fig. 1B for the localization of these sulci). Figure 3 shows maps of both the number of hemispheres with supra-threshold track probabilities (with 3/6 hemispheres as threshold; left maps with cold color code) and the average structural connectivity strength (mean *p-track* with the same threshold; right maps with hot color code). Note that for the very large majority of cortical regions found to connect with pmCSv, the evidence were found in at least 4 hemispheres and thus from all of the individual monkeys. For the few regions with only 3 significant hemispheres, we will specify whenever connectivity could be confirmed in only 2 of the 3 animals.

Whole-Brain Functional Connectivity of pmCSv Based on Resting-State fMRI

In a second step, we used the resting-state fMRI data to create individual whole-brain correlational maps of functional connectivity with left and right pmCSv (Fig. 4A and B, respectively). As in Figure 2, these individual maps are shown on medial and lateral views of the inflated left and right cortical surfaces of our 3 monkeys. In all of them, significant functional connectivity (z-value > 1.96; *P* value < 0.05) again defines a wide network encompassing the temporal, parietal and frontal lobes, and including a large portion of the cingulate cortex. As we observed for the structural connectivity, functional connectivity was found to be very similar between (a) left and

right pmCSv, (b) ipsi- and contralateral hemispheres and (c) the 3 monkeys. Significant negative correlations (z-value > 1.96; *P* value < 0.05) were sometimes observed in the individual maps (Supplementary Fig. 2), but by contrast with the positive ones, they exhibited neither interhemispheric nor interindividual consistency. For that reason, we decided to not consider them further.

The strong reproducibility of the results across monkeys and hemispheres is also demonstrated when projecting all the individual functional connectivity maps onto the flattened and inflated representation of the right cortical surface of the reference monkey F99. Using the same threshold as for structural connectivity (at least 3/6 individual hemispheres with significant connectivity), we show that pmCSv connects functionally with a large number of cortical areas encompassing the cingulate, arcuate, central, intraparietal, lateral and superior temporal sulci, in both ipsilateral (Fig. 5A) and contralateral (Fig. 5B) hemispheres. This is evident in maps plotting the number of hemispheres with supra-threshold/significant functional connectivity (left maps with cold color code) and in maps showing the average functional connectivity strength (mean z-value; right maps with hot color code).

Whole-Brain Convergence of Structural and Functional Connectivity

As a third step, we wished to identify the sites of convergence between structural and functional connectivity with pmCSv. To that end, Figure 6A shows, in red, the cortical regions with supra-threshold structural connectivity at the group level (at least 3/6 hemispheres) and, in green, those with significant functional connectivity (at least 3/6 hemispheres), for both ipsilateral (left maps) and contralateral (right maps) hemispheres. The regions of structural/functional convergence are shown in yellow.
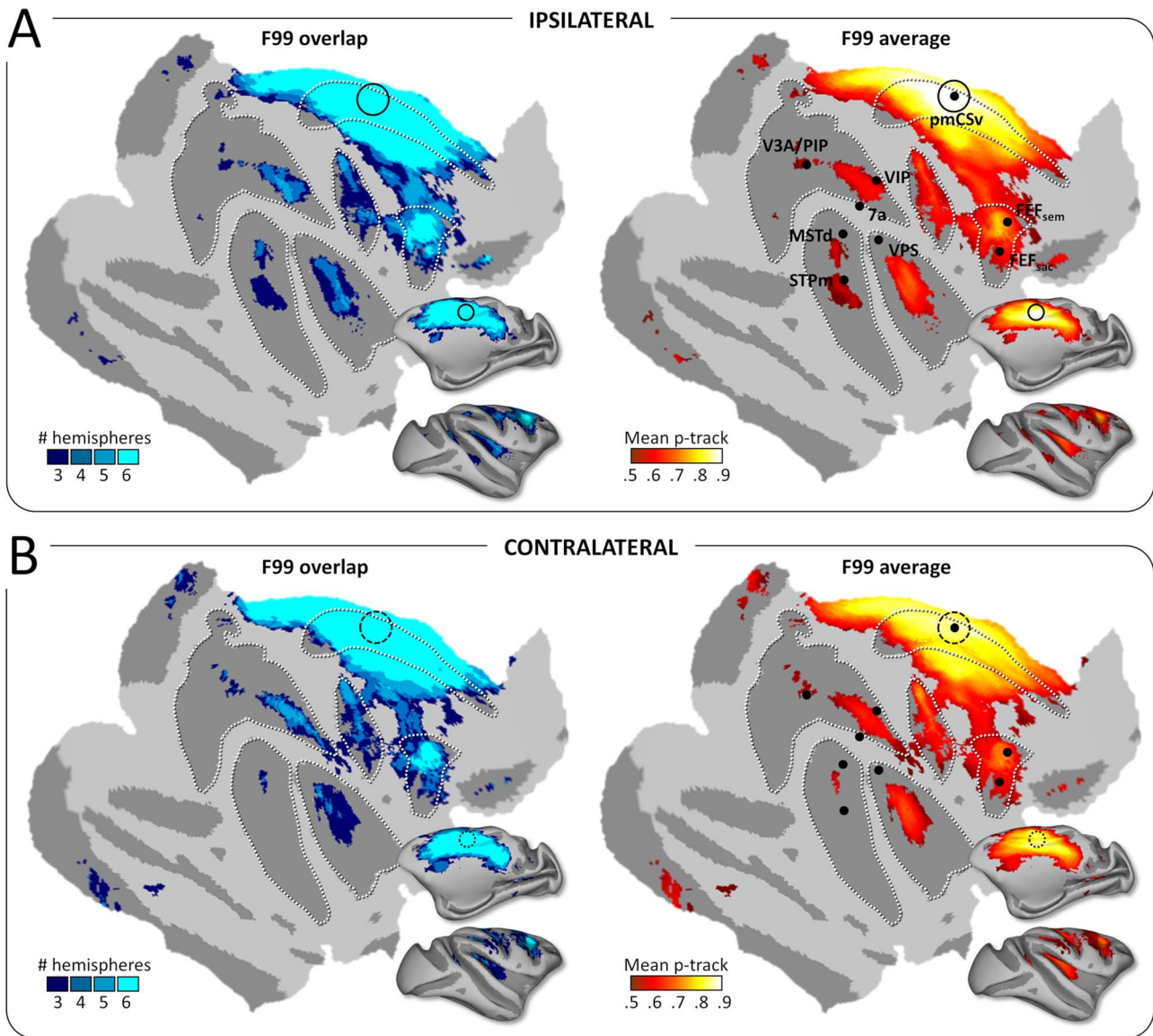
Figure 3. Structural connectivity: group results. Whole-brain pmCSv structural connectivity. Cortical sites showing significant structural connectivity (p-track > 0.5) in at least 3/6 hemispheres (F99 overlap) are shown on the left and the corresponding mean structural connectivity (F99 average) is shown on the right, overlaid in both cases on an inflated and flattened representation of the right cortical hemisphere of monkey F99. (A) Ipsilateral connectivity: tracks of the left pmCSv within left hemisphere and right pmCSv within right hemisphere. (B) Contralateral connectivity: tracks of the left pmCSv with right hemisphere and right pmCSv with left hemisphere. Black dots indicate the local maxima of the responses to egomotion-consistent optic flow stimuli (see Figure 1), with the location of pmCSv signaled by continuous or dotted black circles for the ipsilateral and contralateral pmCSv, respectively. White dotted lines show the delineation of the main sulci.

It can be observed that convergence is found in portions of all the sulci previously identified with both methods separately, namely the cingulate (cis), arcuate (as), central (cs), intraparietal (ips), lateral (ls) and superior temporal (sts) sulci (as labeled in Fig. 1B). However, the structural and functional connectivity patterns of pmCSv are not perfectly overlapping (Fig. 6A). In the posterior cortex (parietal, occipital), functional connections were more dominant. This likely reflects intrinsic properties and limitations associated with the two approaches. Functional connectivity based on resting state (unlike structural connectivity based on diffusion MRI) is partially dependent on the subject's state (Zhang et al. 2019). It is possible that the monkey's state (anesthetized, eyes closed, head restrained) during the functional MR examinations accentuated visual more than

motor connections. Note, however, that anesthetized states tend to produce functional connectivity patterns more closely resembling the structural connectivity (Barttfeld et al. 2015). Moreover, resting-state approaches are more prone to show also indirect connections than structural approaches (Koch et al. 2002).

Structural and Functional Connectivity with Areas Sensitive to Consistent Optic Flow

Interestingly, Figure 6A also reveals that many of the ipsilateral and contralateral sites showing convergence of results between methods closely match with areas previously shown to process visual cues to self-motion in the same animals
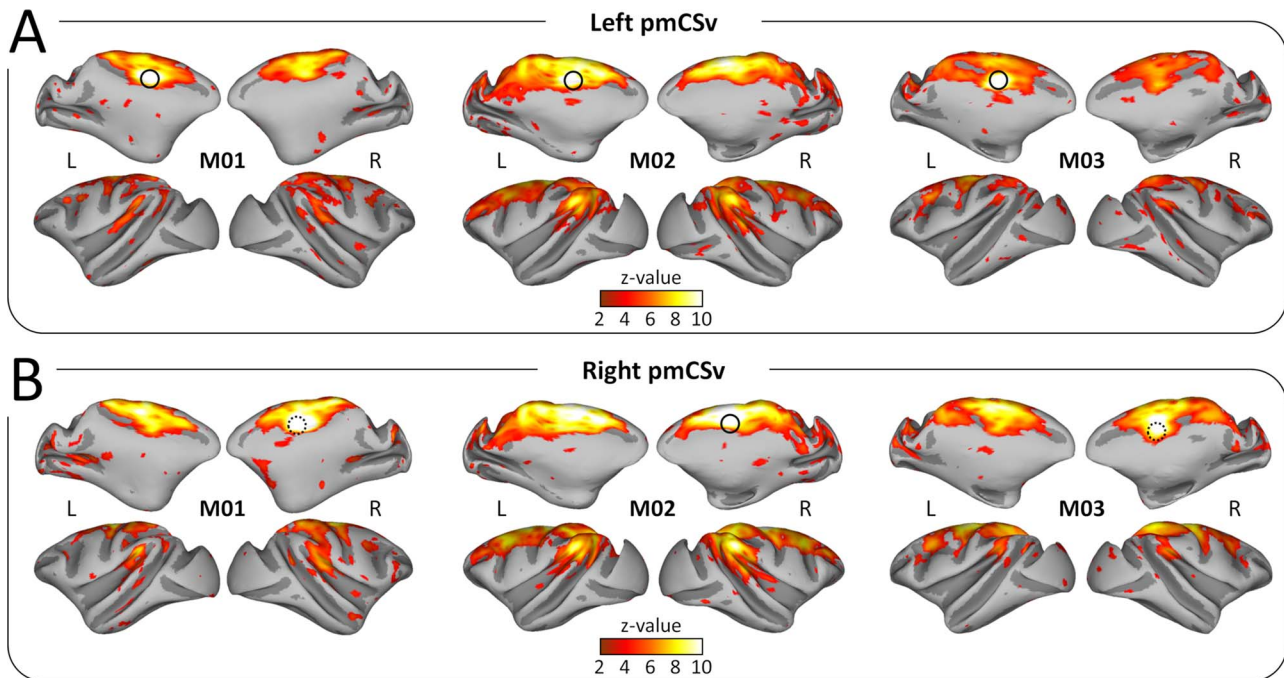
Figure 4. Functional connectivity: individual results. Whole-brain resting-state functional connectivity of the left pmCSv (A) and the right pmCSv (B). Individual z-value maps are projected onto medial and lateral views of the inflated left and right cortical surfaces for the 3 monkeys (threshold: z-value > 1.96).

(Cottereau et al. 2017). This is unsurprising for pmCSv, but it holds for areas, which are relatively far apart, such as VIP, FEFsem, and MSTd. To further investigate the structural and functional connectivity of pmCSv with areas sharing its responsiveness to visual cues to self-motion, we performed additional ROI-based analyses in the structural and functional domains (see Methods section). Following Smith et al. (2018), the mean connectivity across the early visual areas V1/V2/V3 was used as a baseline, since neither the human CSv nor its putative monkey counterpart are expected to have direct connections with them. In the structural domain, the upper graph (in red) of Figure 6B indicates that most areas previously identified for their sensitivity to visual cues to self-motion (MSTd, STPm, VIP, VPS, FEFsem and FEFsac) were more connected to pmCSv than to the early visual cortex. This was also the case for the newly identified portion of V3A/PIP. A notable exception is area 7a/Opt, whose mean structural connectivity was similar to that of V1/V2/V3 (dashed horizontal line). In the functional domain, the lower graph (in green) of Figure 6B reveals a very similar pattern of results, with the majority of ROIs highly connected to pmCSv compared to V1/V2/V3. Here, however, 7a/Opt was found to be functionally connected to pmCSv while STPm was not (relative to V1/V2/V3). Note that for all these ROIs, the relative strengths of structural and functional connectivities were strikingly similar between the ipsilateral (black circles) and contralateral (white circles) hemispheres. Note also that the analyses were performed in the surface space of the right cortex of monkey F99, after projection of the individual ROIs onto it. However, our control analyses showed (1) that the structural connectivity results were similar when running the ROI-to-ROI analysis in the initial volumetric diffusion MRI space (Supplementary Fig. 3A) and (2) that the functional connectivity results were also reproducible when splitting the odd and even runs acquired with resting-state fMRI (Supplementary Fig. 3B).

Finally, Figure 6C shows that when translated into *t*-values (see Methods), the structural and functional connectivity strengths are well correlated, pointing to VIP and FEFsem as the areas most strongly connected to pmCSv, followed by MSTd, FEFsac, VPS and V3A/PIP. Note that these optic flow sensitive areas were systematically identified in all 3 animals (see Table 1 in Cottereau et al. 2017). Since we could also localize area V6 in 2 of the 3 animals, we extended our ROI-based analysis to this area, which is one of the more strongly connected with CSv in humans (Smith et al. 2018). As shown in Supplementary Figure 4, the portions of area V6 sensitive to egomotion-consistent optic flow in M01 and M02 (Supplementary Fig. 4A) have no significant structural connectivity with pmCSv (Supplementary Fig. 4B) and only moderate functional connectivity, mostly driven by M02 (Supplementary Fig. 4C). This analysis confirms a marked difference between human V6 and its monkey counterpart, since the latter is neither strongly responsive to egomotion-consistent optic flow patterns, nor clearly connected to pmCSv.

Structural and Functional Connectivity with Whole-brain Atlas-Defined Areas

Our last analysis extended the ROI-based approach described above to an extensive set of atlas-defined areas covering the whole cortical surface. We relied on the cortical parcellation introduced by Markov and collaborators (2014), based on histological (Markov et al. 2011) and atlas-based (Paxinos et al. 2000; Saleem and Logothetis 2007) landmarks, which contains 91 distinct areas already available on the reference monkey F99 (see Fig. 7C for the parcellation scheme on top of the flattened right cortical surface of F99). Profiles of structural and functional connectivity strengths (mean *p*-tracks and mean Fisher Z-transformed *r*-values across the 6 ipsilateral and 6 contralateral hemispheres) are shown in Figure 7A for all these areas, with
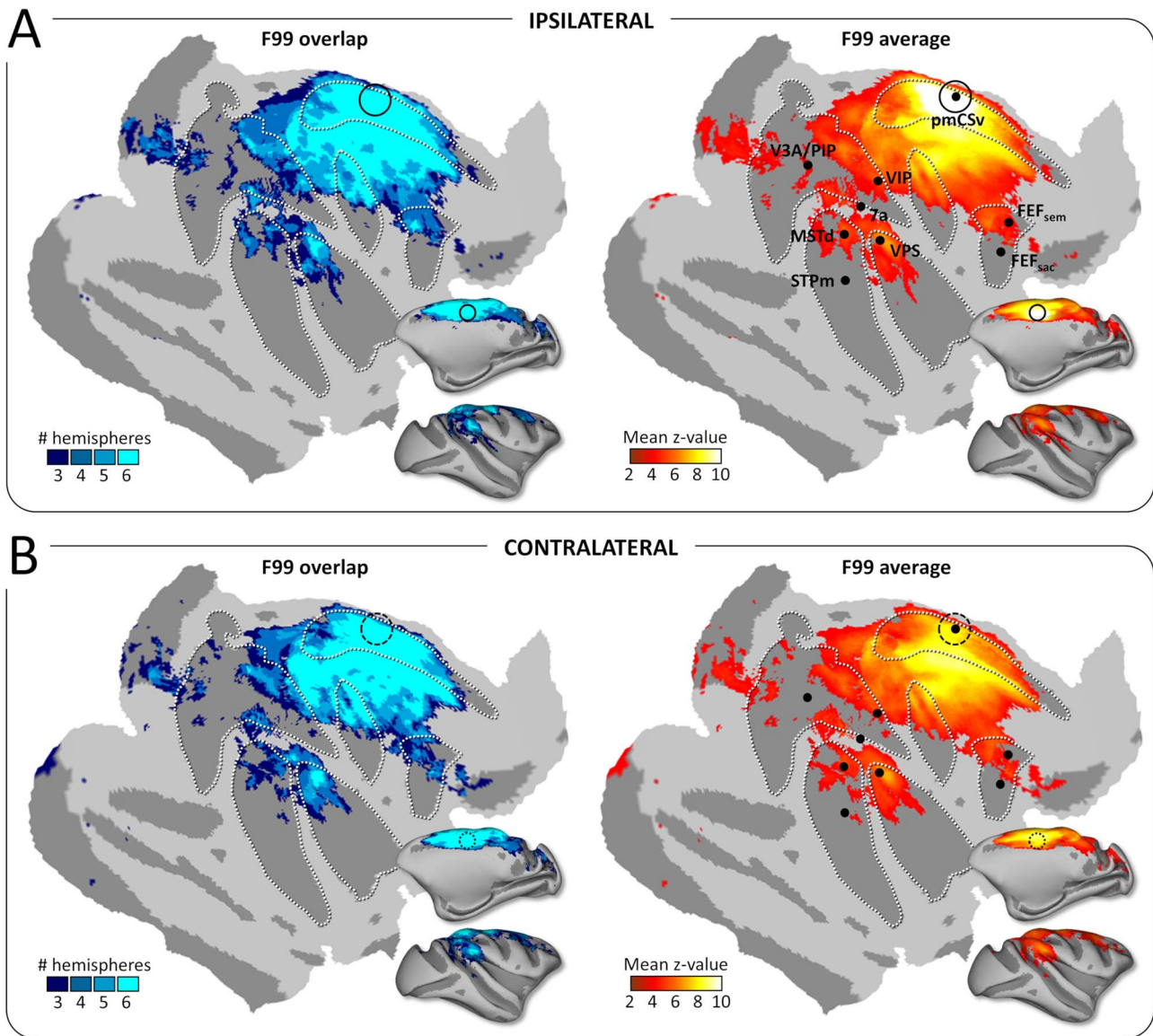
Figure 5. Functional connectivity: group results. Whole-brain pmCSv resting-state functional connectivity. Cortical sites showing significant functional connectivity (z-value > 1.96) in at least 3/6 hemispheres (F99 overlap) are shown on the left and the corresponding mean functional connectivity (F99 average) is shown on the right, overlaid in both cases on an inflated and flattened representation of the right cortical hemisphere of monkey F99. (*A*) Ipsilateral connectivity: mean z-values of the left pmCSv within left hemisphere and right pmCSv within right hemisphere. (*B*) Contralateral connectivity: mean z-values of the left pmCSv with right hemisphere and right pmCSv with left hemisphere. Black dots indicate the local maxima of the responses to egomotion-consistent optic flow stimuli (see Figure 1), with the location of pmCSv signaled by continuous or dotted black circles for the ipsilateral and contralateral pmCSv, respectively. White dotted lines show the delineation of the main sulci.

the mean connectivity strengths of V1/V2/V3 (horizontal dashed lines) used as a baseline for statistical evaluation. In total, 20 of these areas exhibited both significantly stronger structural connectivity and stronger functional connectivity with pmCSv than that measured for V1/V2/V3 areas, as shown with the t-value statistics of Figure 7B (t-value > 2.6 for both structural and functional connectivity; p-value $< 10^{-4}$ for combined probability). These 20 areas are color coded from blue to yellow in Figure 7B and C, depending on the normalized combined connectivity strength (see Methods section).

Table 1 provides summary statistics for these 20 areas, that can roughly be classified as visual or visuo-vestibular (7 m, 7op, 8 m, VIP, Tpt, MST, LIP, MT, V6), somatosensory or

visuo-somatosensory (areas 1, 3 and 2, STPc) and (pre)motor (23, F3, 24d, F1, F2, F4, F6). In the visual and visuo-vestibular domains, this atlas-based analysis both confirms and extends the results obtained with regions sensitive to visual cues to self-motion that were identified in the same 3 animals (Cottereau et al. 2017). Notably, VIP was found to be strongly connected to pmCSv with both analyses, and the same holds for FEFsem (whose location matches that of 8 m in the atlas), VPS (in close correspondence with area 7op in the atlas), and MSTd (matching the atlas-defined MST). In addition, the atlas-based analysis reveals strong pmCSv connections with the medial posterior parietal area 7 m (also known as PGm), which has been shown to be involved in navigation (Passarelli et al. 2018), and residual
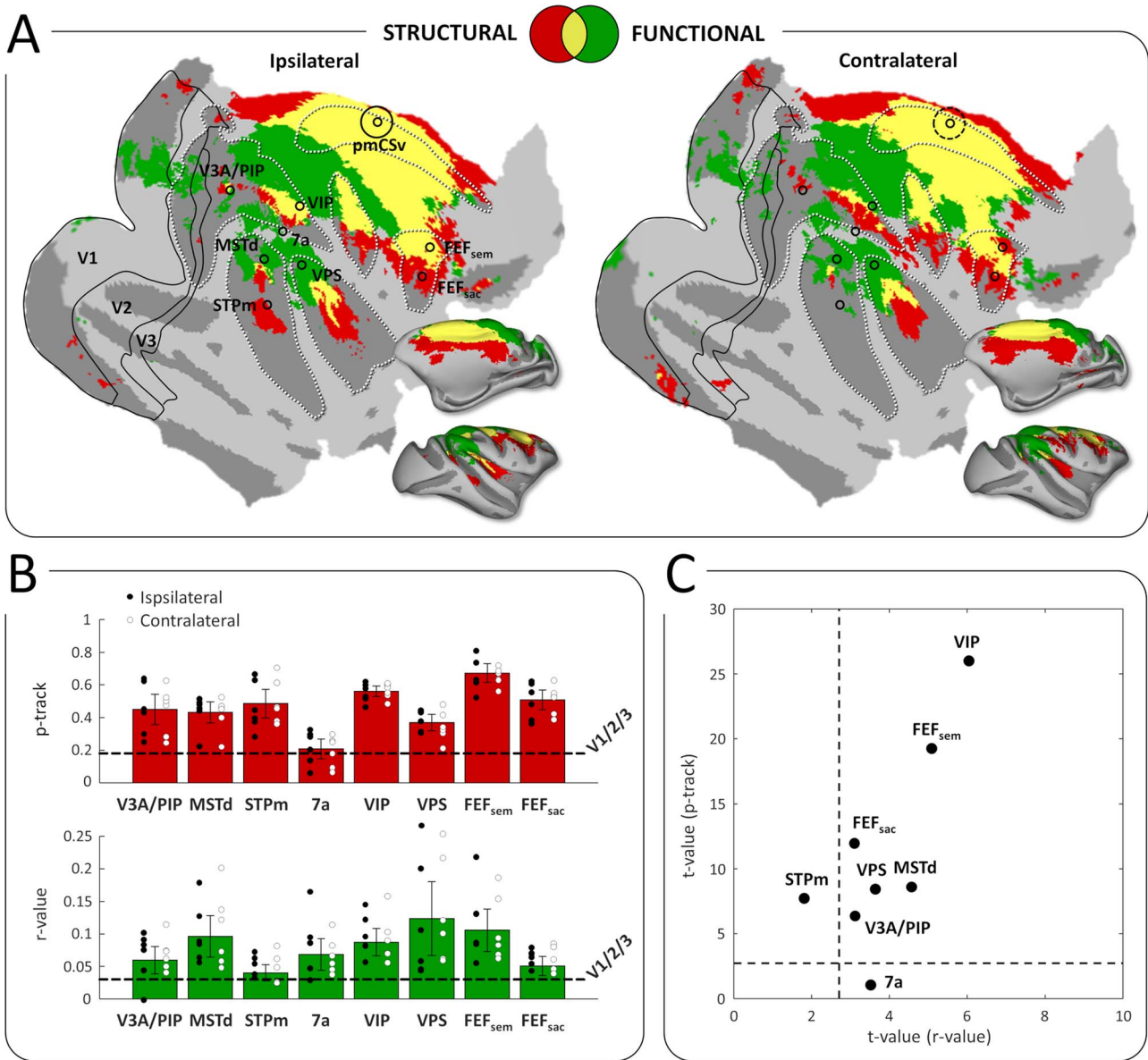
Figure 6. Conjunction of functional and structural connectivity. (A) Overall maps of pmCSv connectivity, with structural connectivity only (in red), functional connectivity only (in green), or both types of connectivity (in yellow), projected on flattened and inflated representations of the right cortical hemisphere of monkey F99. Maps of ipsilateral and contralateral connectivity are shown on the left and right sides, respectively. Regions that are specifically activated by egomotion-consistent optic flow are indicated: V3A/PIP, MSTd, STPm, 7a, VIP, VPS, FEFsem, FEFsac (Figure 1). Borders of the visual areas V1, V2, and V3 are shown as black lines. Black circles indicate the local maxima of the responses to egomotion-consistent optic flow stimuli (Figure 1), with the location of pmCSv signaled by continuous or dotted black circles for the ipsilateral and contralateral pmCSv, respectively. White dotted lines show the delineation of the main sulci. (B) Bar graphs of pmCSv mean structural (track probabilities; in red) and functional (correlation coefficients; in green) connectivity (with 95% confidence intervals) with each of the target areas marked in (A). The horizontal dashed lines represent the average results of V1/V2/V3 for statistical comparison. Individual results are shown as black and white dots for ipsilateral and contralateral connectivity respectively. (C) Scatterplot showing the strength of the structural and functional connectivity for all the target areas relative to the mean connectivity of V1/V2/V3, expressed as t-values. The dotted lines indicate the threshold of statistical significance (t-value>2.6; $P < 0.05$).

but significant structural and functional connections with areas MT and V6, both known to play a central role in the processing of visual motion (Passarelli et al. 2011; Fan et al. 2015). Regarding the connections of pmCSv with somatosensory areas on the one hand, and with (pre)motor areas of the cingulate and dorsal prefrontal cortex on the other hand, both of them are highly reminiscent of the connectivity pattern described for human CSv (Smith et al. 2018).

The scatter plot of t-values in Figure 7B also shows several brain areas with negative t-values (bottom-left corner of the plot), suggesting less connectivity with pmCSv than between V1/V2/V3 and pmCSv. On the one hand, this confirms that our baseline (V1/V2/V3) is indeed a conservative threshold. A conservative threshold is needed in order to protect our analysis against false positives. Note, however, that this means that the plotted connectivity measures reflect relative rather than
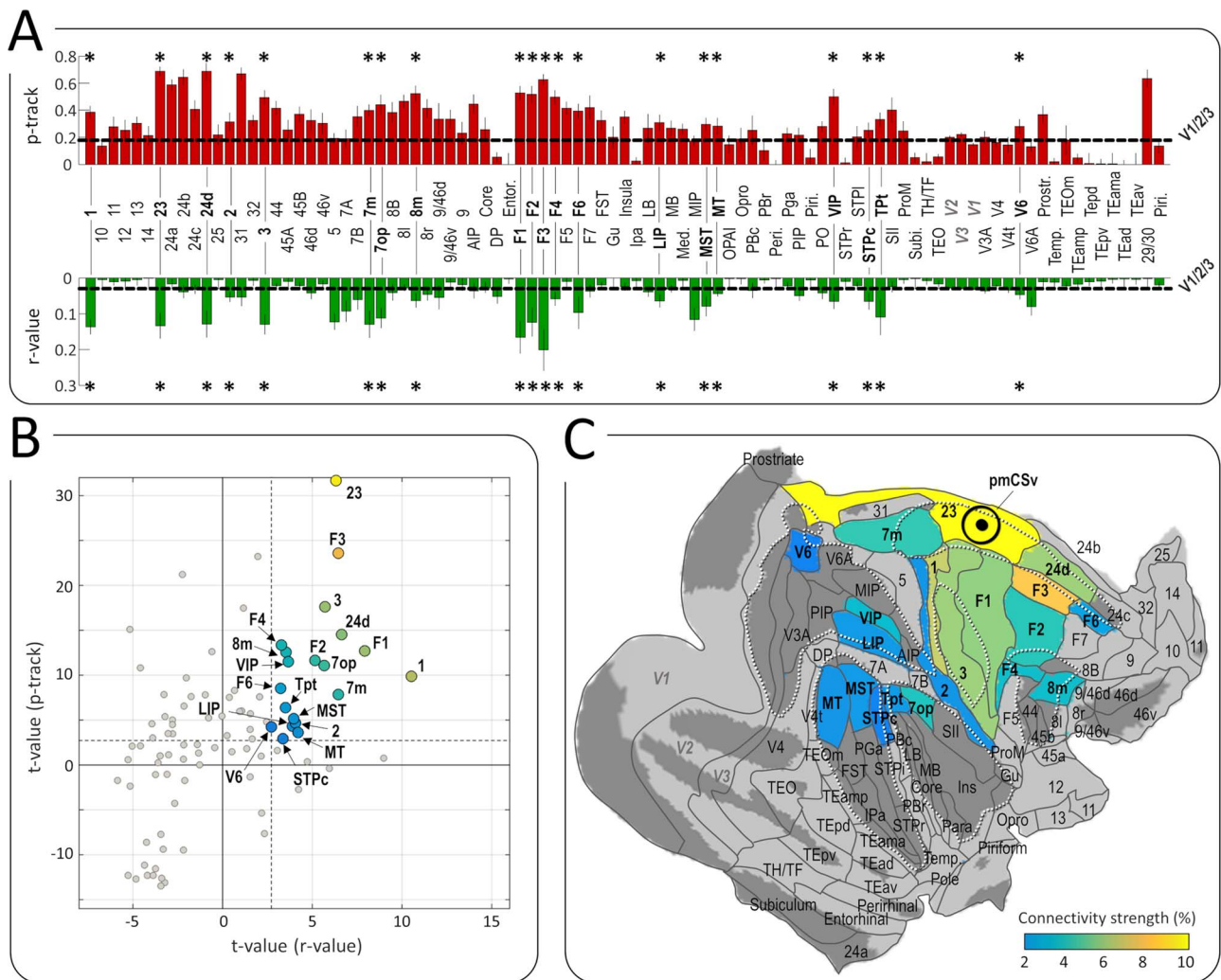
Figure 7. Whole-brain atlas-based analysis of structural and functional connectivity. (A) Profiles of structural (in red) and functional (in green) connectivity scores for the areas of the M132 atlas (Markov et al. 2014). The horizontal dashed lines represent the average results of V1/V2/V3. Asterisks indicate the areas for which the structural and functional connectivity are significantly stronger than that of reference areas V1/V2/V3 (t-value > 2.6; P < 0.05). (B) Scatter plot of structural and functional t-values for the 20 areas showing significant connectivity (t-value > 2.6 as indicated by dashed lines) with pmCSv. Gray dots represent the t-values of the remaining areas. Negative values represent areas with lower connectivity strength than the reference areas (V1/V2/V3). (C) The 91 areas of the M132 atlas registered onto the right cortical surface of monkey F99. The 20 areas color-coded from blue to yellow (according to the normalized average of their t-values for functional and structural connectivity; i.e., their connectivity strength, see Methods) are those showing statistically stronger structural and functional connectivity with pmCSv than areas V1/V2/V3. White dotted lines show the delineation of the main sulci. See also Supplementary Table 1.

absolute levels of connectivity. On the other hand, it is possible that early visual areas (V1/V2/V3), unlike previously thought, might be connected to pmCSv either by direct or indirect connections. The whole-brain connectivity maps (Fig. 5) suggest that at least small portions of V1/V2/V3 are functionally connected with pmCSv. Most of the visual input to CSv and related self-motion-sensitive areas can be assumed to derive in some way from activity in V1 (principally via its projection to MT) so some degree of connectivity with V1, mediated by indirect connections, is expected. V2 and V3 both have projections to MT (Felleman et al. 1997; Gattass et al. 1997) and may also be involved; in humans, global motion direction can be decoded in both these areas (Furlan and Smith 2016). Data from the structural and functional connectivity strength (mean and SD) between pmCSv and all the atlas-defined areas are shown in Supplementary Table 1.

Discussion

The major aim of the present study was to investigate the connectivity of pmCSv, a region that has recently been identified in macaques (Cottereau et al. 2017), and which might represent the functional equivalent of human CSv (Wall and Smith 2008). Recently, the connectivity of human CSv was examined in detail using two different strategies, (1) the study of its structural connections based on diffusion-weighted MRI and (2) the study of its functional connections based on resting-state fMRI (Smith et al. 2018). Here, we have implemented a comparable procedure in 3 macaques in order to investigate the connectivity of pmCSv with that of human CSv. First, we analyzed the whole-brain patterns of structural and functional connectivity in order to localize the cortical regions connected with pmCSv. The two connectivity approaches resulted in broadly converging

evidence. Secondly, we made ROI to ROI analyses for the purpose of studying more specifically the connections of pmCSv with areas sensitive to self-motion-consistent optic flow. Thirdly, we conducted an exhaustive atlas-based analysis. Essentially, our results show that pmCSv connects structurally and functionally with several visual and/or vestibular areas, as well as with somatosensory areas. Besides those (multi)sensory areas, pmCSv was also found to connect strongly with (pre)motor areas of the anterior cingulate and dorsal prefrontal cortices. This connectivity pattern presents many commonalities with that documented for human CSv, though with some exceptions, and it suggests that in both species, this area might play a central role in the sensorimotor control of locomotion. In the following paragraphs we will discuss in more detail the visuo-vestibular, somatosensory and (pre)motor connections of pmCSv.

Connectivity of pmCSv with Visual and/or Vestibular Areas

The convergence of structural and functional connectivity reveals that pmCSv is connected with most of the regions that were previously shown to respond to egomotion-consistent optic flow (Cottereau et al. 2017). The strongest of these connections were observed for VIP and FEFsem (Fig. 6C). Significant connectivity was also evident for VPS and MSTd. These results are largely confirmed by the atlas-based analysis (Fig. 7), where FEFsem likely corresponds to area 8 m (Babapoor-Farrokhran et al. 2013) and VPS to 7op (Chen et al. 2011a). All four regions have been shown to process both visual and vestibular inputs (Schlack et al. 2002; Gu et al. 2008, 2016; Chen et al. 2011a, 2011b), indicating that pmCSv has access to both types of self-motion cue. Note that for VIP and FEFsem/8 m, the *t*-values of structural and functional connectivity were much higher in the ROI-based than in the atlas-based analysis. This suggests that these atlas-based areas may not be functionally homogeneous but rather may comprise different zones with different sensitivities, in which case the connectivity with pmCSv might target mostly those portions that are sensitive to self-motion-consistent optic flow.

Besides those connections, the atlas-based analysis reveals a strong connection between pmCSv and the medial posterior area 7 m/PGm (Table 1 and Fig. 7). This observation fits with previous anatomical studies that documented projections from 7 m/PGm to area 23, where pmCSv is located (Leichnetz 2001; Passarelli et al. 2018). Area 7 m/PGm receives strong inputs from V6A (Passarelli et al. 2011) as well as from other visuomotor areas such as FEFsem, MST, and LIP, which has led to postulate its involvement in visuospatial cognition and notably navigation (Passarelli et al. 2018). Interestingly, the same group (Passarelli et al. 2011) has previously shown that area 23 does not connect to V6A, which is also in agreement with our results.

Our atlas-based analysis also shows that pmCSv has low-strength connections with LIP, V6 and MT. However, none of these areas exhibit clear-cut preference for egomotion-consistent over inconsistent optic flow stimuli (Cottereau et al. 2017) nor any special sensitivity to vestibular signals (Colby et al. 1993; Fan et al. 2015). Altogether, these observations raise the possibility that the underlying connections may be indirect, through MSTd or VIP for instance (Boussaoud et al. 1990; Shipp et al. 1998; Galletti et al. 2001) and that the weak connectivity of these areas with pmCSv may be of limited functional significance.

In humans, the structural and functional connectivity of CSv points to hV6, hVIP, and PIC as the most important sources of visual and/or vestibular information, with an additional potential contribution of hMST and V3A (Smith et al. 2018). Assuming a functional equivalence between monkey VPS and human PIC (Chen et al. 2011b; Frank et al. 2014; Wirth et al. 2018), the commonalities between both primate species are significant. A notable difference is area V6. In humans, hV6 was found to be among the areas most strongly connected to CSv, while in monkeys, the V6/pmCSv connection, is the weakest in our analysis (see Table 1) and it was not confirmed in the ROI-based analysis (see Supplementary Fig. 4). Importantly, this difference echoes that already documented regarding their respective sensitivities to egomotion-consistent optic flow stimuli, which is strong in human hV6 (Cardin and Smith 2010) but weak in monkey V6 (Cottereau et al. 2017). The fact that a species difference in relation to V6 is evident for both visual sensitivity and connectivity suggests strongly that the difference is real. A comprehensive cross-species comparison of sensitivity to visual/vestibular cues to self-motion in different cortical regions has been provided by Smith et al. (2017).

Connectivity of pmCSv with Somatosensory Areas

Our whole-brain analysis reveals a convergence of structural and functional connectivity for pmCSv with the anterior and posterior banks of the central sulcus (Fig. 6A), which are involved in motor and somatosensory functions, respectively. Regarding the somatosensory connections, the atlas-based analysis further confirmed strong connectivity with the somatosensory areas 1 and 3, and to a lesser extent with area 2 (Fig. 7B and C). Although the somatosensory cortex handles all sorts of somatic signals, it has notably been shown to process those triggered by locomotion in humans (la Fougère et al. 2010), monkeys (Fitzsimmons et al. 2009), and other mammals (Chapin and Woodward 1982; la Fougère et al. 2010; Favorov et al. 2015; Karadimas et al. 2020). In addition, pmCSv was also found to connect structurally and functionally with the caudal portion of the superior temporal polysensory (cSTP) area, which is also known to process somatosensory and visual information (Bruce et al. 1981; Hikosaka et al. 1988). By showing that pmCSv is linked to visual, vestibular and somatosensory areas, our results reinforce the idea that this posterior cingulate area integrates signals from various sensory modalities recruited during self-motion.

Connectivity of pmCSv with Motor and Premotor Areas

According to the atlas delineation, pmCSv belongs to a subdivision of cingulate area 23 (Fig. 7C) called 23c, within the ventral bank of the cingulate sulcus (Vogt et al. 1987). Area 23c also houses a motor area known as the ventral cingulate motor area CMAv (Picard and Strick 1996), which might well correspond to pmCSv. Alternatively, pmCSv might be posterior to CMAv and connect to that latter as it does with other premotor areas of the hemispheric medial wall (Matelli et al. 1991), that is, area 24d (also called rostral cingulate motor area, CMAr) and F3 (the supplementary motor area, SMA). Interestingly, microstimulation of F3 and 24d evokes both hindlimb and forelimb movements (Luppino et al. 1991). The exact role of these areas is uncertain but, given their connectivity with pmCSv, it is possible that their motor functions are entirely or predominantly locomotion related. Two lateral premotor areas were also found to have
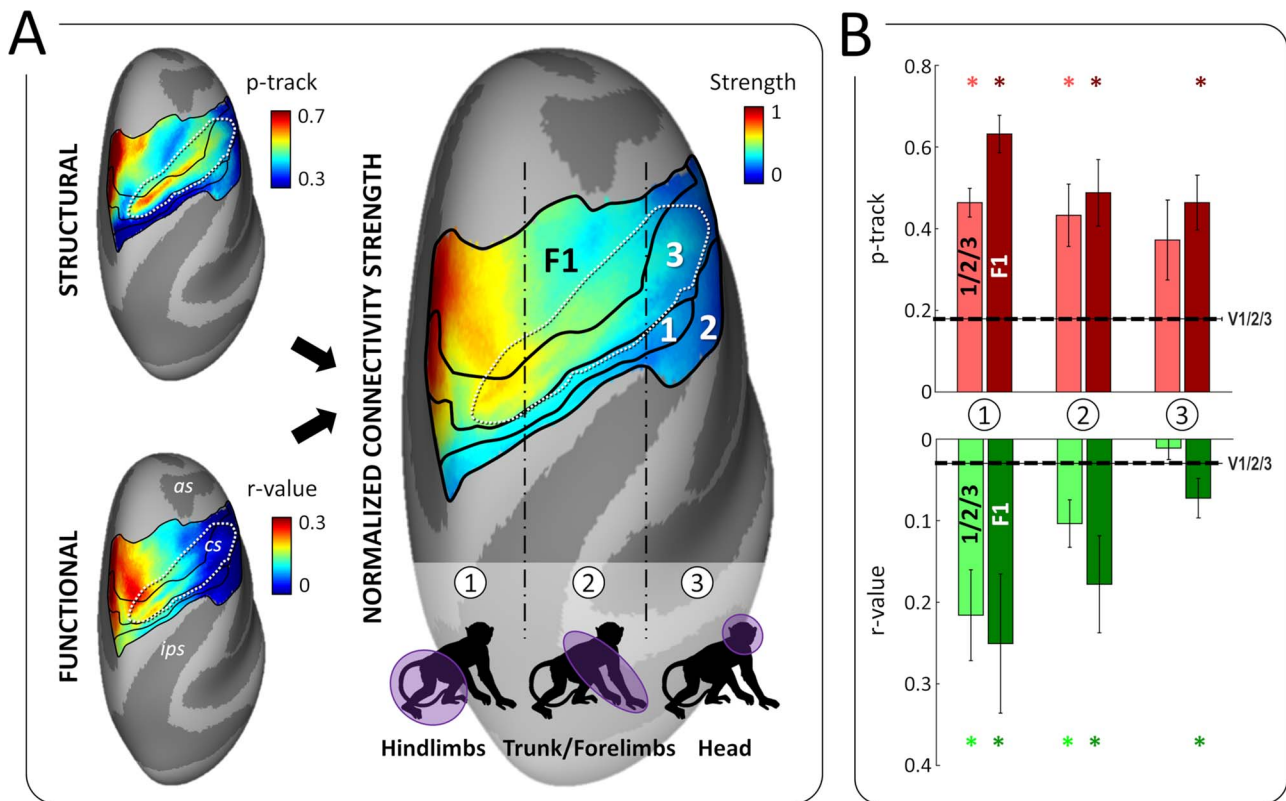
Figure 8. Connectivity of pmCSv with the somatosensory and motor cortices. (A) Somatosensory areas 2, 1 and 3 lie along the postcentral gyrus and the posterior bank of the central sulcus (cs), while the motor area F1 occupies the anterior bank of the cs and the precentral gyrus. Both the somatosensory and motor cortices have a roughly similar somatotopic organization, from the feet/hindlimbs medially to the head laterally, passing by the trunk and forelimbs in-between. Maps of structural and functional connectivity between these regions and pmCSv are shown on the left, on inflated representations of the F99 monkey's right cortical surface. These maps were normalized and averaged to produce a map of overall connectivity strength, displayed on the right. Thus, connectivity is the strongest for the hindlimbs, intermediate for the trunk/forelimbs and virtually absent for the head. Note that among the somatosensory areas, area 3 is the most strongly connected with pmCSv. (B) Strength of structural (in red) and functional (in green) connectivity in the medial (1), intermediate (2) and lateral (3) sectors of somesthetic areas 1/2/3 (pale colors) and motor F1 area (dark color). Bars and error bars indicate the means and related 95% CI across the 6 ipsilateral and 6 contralateral hemispheres. Stars signal significant structural and functional connectivity with respect to the V1/V2/V3 baseline.

strong ties with pmCSv: the dorso-caudal area F2 (PMDc) and the ventrocaudal area F4 (PMVc). No significant connectivity was found with the dorso-rostral area F7 (PMDr) or the ventro-rostral area F5 (PMVr). Caudal premotor areas connect predominantly with the parietal cortex and posterior cingulate cortex, and they are thought to be involved in sensorimotor transformations and online motor control. By contrast, rostral areas connect mostly with the prefrontal and anterior cingulate cortices and they have been implicated in more cognitive operations linked to motivation, memory and long-term motor plans (see Rizzolatti and Luppino 2001 for review). Thus, the fact that pmCSv only connects with caudal premotor areas reinforces the view that it is involved in the online control of locomotion. This pattern of results is strikingly similar to that evidenced in human CSv with the same approach, as CSv was shown to connect with cingulate motor areas, the SMA and probably some other premotor areas belonging to Brodmann area 6 (Smith et al. 2018). The human cingulate cortex appears to contain multiple small regions that are active during motor activity, and it has been suggested, based on fMRI studies, that these can reliably be grouped into three clusters that might correspond to macaque CMAv, CMAd, and CMAr (Amiez and Petrides 2014; Loh et al. 2018). Weaker connections were also observed with F6, which has been described as

the pre-SMA (Luppino et al. 1991). As revealed here for pmCSv, all these premotor areas have been shown to have direct connections with the primary motor area F1 (Picard and Strick 1996; Rizzolatti and Luppino 2001 for reviews).

In general, we observe that the strongest connectivity of pmCSv is with motor and somatosensory areas rather than with visuo-vestibular areas (see Table 1 and Fig. 7). This is also true of human CSv (Smith et al. 2018). This suggests that pmCSv is perhaps best viewed as a sensorimotor area that exploits sensory information for online motor control, rather than as the visuo-vestibular area originally described (Wall and Smith 2008).

Somatotopy-Dependent Connectivity of pmCSv with Somatosensory and Motor Cortices

In humans, CSv has been found to connect predominantly with the somatosensory representations of the legs and feet (Smith et al. 2018) and recently, Serra and collaborators (2019) reported that active leg movements trigger CSv activations (together with activations of the posterior insular and posterior cingulate sulcus areas). It is tempting to consider these results as evidence that CSv serves the sensorimotor control of our bipedal locomotion. Alternatively, one might also speculate a more general
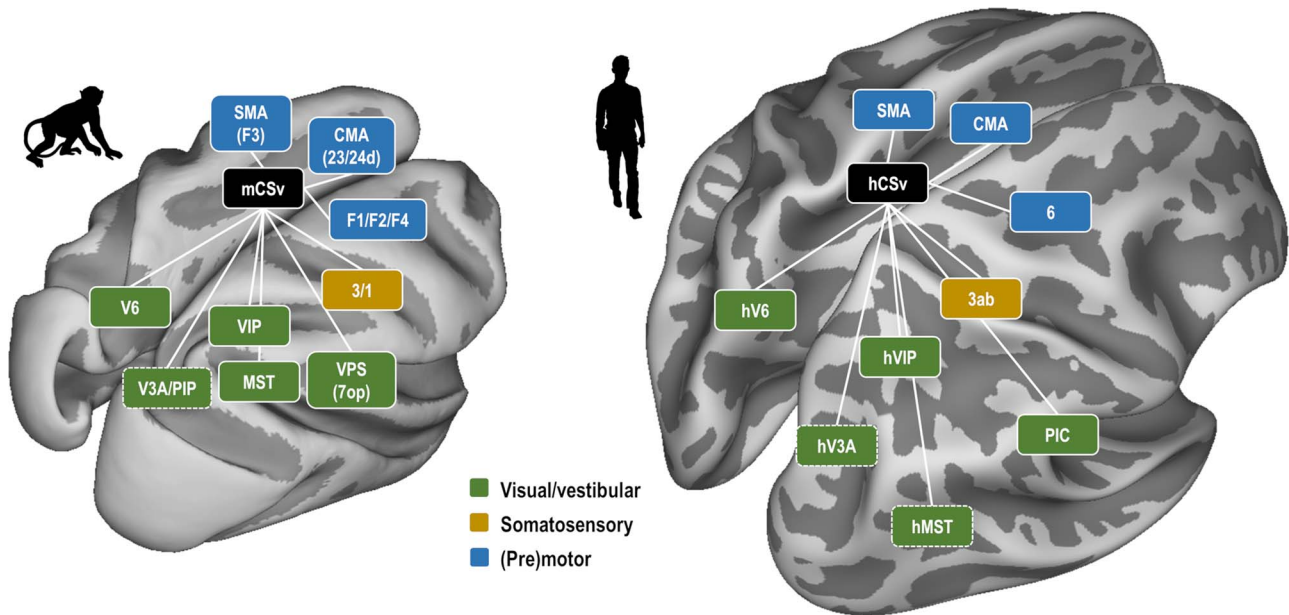
Figure 9. Commonalities in the connectivity patterns of monkey CSv (mCSv) and human CSv (hCSv). In both primate species, CSv connects with a set of visual and visuo-vestibular areas (green) largely sensitive to self-motion-consistent optic flow stimuli. Connections are also found with the somatosensory cortex, and mostly area 3 (orange). Finally, CSv is strongly connected with several (pre)motor areas (blue): cingulate (pre)motor areas (CMA), the supplementary motor area (SMA/F3) and other dorsal premotor areas belonging to Brodmann area 6. Areas surrounded by dotted lines indicate those for which evidences were not fully consistent across imaging (structural/functional) or analytical (ROIS-based/Atlas-based) approaches.

involvement in the control of actions involving the legs. By contrast with humans, the locomotion of macaque monkeys is quadrupedal (Colin 2005), with forelimbs and hindlimbs of similar length to enable more energy-efficient movement on a terrestrial substrate (Kimura 1992; Roos and Zinner 2015). Thus, if CSv is specifically involved in the control of locomotion in both primate species (rather than in the more general control of actions involving the legs), one might expect that in macaques, it connects not only to sensorimotor representations of the feet and hindlimbs, but additionally to those of the trunk and forelimbs. Although we did not perform somatotopic mapping in our animals, a rough approximation is that the medio-dorsal third is dedicated to the feet and hindlimbs, the central third represents the trunk and forelimbs and the latero-ventral third is related to the face (Delhaye et al. 2018; Arcaro et al. 2019). As shown in Figure 8A, both the somatosensory areas (1/2/3) and primary motor cortex (F1) exhibit a marked medio-lateral connectivity gradient in the structural and functional domains. Combining them after normalization produces an overall connectivity strength that is maximal medio-dorsally and decreases to a minimum latero-ventrally. However, significant functional and structural connectivity is found at least up to the trunk and forelimb representations, in both somatosensory and motor domains (Fig. 8B). These results represent a further argument for the involvement of CSv in the online control of locomotion in both human and nonhuman primates.

Note that in humans, the absence of connectivity between CSv and sensorimotor representations of the trunk seems to contradict the important role of the latter during locomotion (Anson et al. 2014). It might be that CSv participates in monitoring, computing or maintaining the direction of self-motion, but not necessarily in postural stability during locomotion.

Conclusion

By using diffusion MRI and rs-fMRI, we characterized the structural and functional connectivity of the putative monkey counterpart of human CSv. We identified the links of pmCSv with a set of areas processing visual and vestibular cues to self-motion, from which it probably inherits its sensitivity to egomotion-consistent optic flow stimuli (Cottereau et al. 2017). In addition, we found that pmCSv was strongly connected with somatosensory areas and with (pre)motor areas of the cingulate and prefrontal cortices. Somatosensory and motor connections are organized somatotopically, targeting primarily the hindlimb, trunk and forelimb representations. As shown in Figure 9, these results are reminiscent of those recently documented for human CSv (Smith et al. 2018), indicating that the similarities with monkey CSv extends far beyond a common sensitivity to visual cues to self-motion. In both species, the sensory and motor connections of this cingulate area suggest that it is involved in the sensorimotor online control of locomotion, possibly among other types of actions involving the hindlimbs, trunk and forelimbs. Thus, although numerous anatomical markers reflect radical differences in the locomotor habits of humans and macaque monkeys, the cortical control of locomotion in both primate species appears to rely on a highly preserved functional organization.

Supplementary Material

Supplementary material can be found at *Cerebral Cortex* online.

Acknowledgements

Funding

References

Amberg B, Romdhani S, Vetter T. 2007. Optimal step non-rigid ICP algorithms for surface registration. In: *Proceedings of the IEEE Computer Society Conference on Computer Vision and Pattern Recognition*. Minneapolis, MN, pp. 1–8. doi: 10.1109/CVPR.2007.383165.

Amiez C, Petrides M. 2014. Neuroimaging evidence of the Anatomo-functional Organization of the Human Cingulate Motor Areas. *Cereb Cortex*. 24:563–578.

Andersson JLR, Skare S, Ashburner J. 2003. How to correct suscep-tibility distortions in spin-echo echo-planar images: applica-tion to diffusion tensor imaging. *Neuroimage*. 20:870–888.

Andersson JLR, Sotiropoulos SN. 2016. An integrated approach to correction for off-resonance effects and subject movement in diffusion MR imaging. *Neuroimage*. 125:1063–1078.

Anson E, Agada P, Kiemel T, Ivanenko Y, Lacquaniti F, Jeka J. 2014. Visual control of trunk translation and orientation during locomotion. *Exp Brain Res*. 232:1941–1951.

Antal A, Baudewig J, Paulus W, Dechent P. 2008. The poste-rior cingulate cortex and planum temporale/parietal oper-culum are activated by coherent visual motion. *Vis Neurosci*. 25:17–26.

Arcaro MJ, Schade PF, Livingstone MS. 2019. Body map proto-organization in newborn macaques. *Proc Natl Acad Sci USA*. 116:24861–24871.

Babapoor-Farrokhran S, Hutchison RM, Gati JS, Menon RS, Ever-ling S. 2013. Functional connectivity patterns of medial and lateral macaque frontal eye fields reveal distinct visuomotor networks. *J Neurophysiol*. 109:2560–2570.

Barttfeld P, Uhriga L, Sitta JD, Sigmane M, Jarrayaa B, Dehaene S. 2015. Signature of consciousness in the dynamics of resting-state brain activity. *Proc Natl Acad Sci U S A*. 112:887–892.

Beer AL, Plank T, Greenlee MW. 2011. Diffusion tensor imaging shows white matter tracts between human auditory and visual cortex. *Exp Brain Res*. 213:299–308.

Behrens TEJ, Berg HJ, Jbabdi S, Rushworth MFS, Woolrich MW. 2007. Probabilistic diffusion tractography with multiple fibre orientations: what can we gain? *Neuroimage*. 34:144–155.

Behrens TEJ, Johansen-Berg H, Woolrich MW, Smith SM, Wheeler-Kingshott CAM, Boulby PA, Barker GJ, Sillery EL, Sheehan K, Ciccarelli O et al. 2003. Non-invasive mapping of connections between human thalamus and cortex using diffusion imaging. *Nat Neurosci*. 6:750–757.

Boussaoud D, Ungerleider LG, Desimone R. 1990. Pathways for motion analysis: cortical connections of the medial superior temporal and fundus of the superior temporal visual areas in the macaque. *J Comp Neurol*. 296:462–495.

Bremmer F, Klam F, Duhamel J-R, Ben Hamed S, Graf W. 2002. Visual-vestibular interactive responses in the macaque ven-tral intraparietal area (VIP). *Eur J Neurosci*. 16:1569–1586.

Bremmer F, Schlack A, Shah NJ, Zafiris O, Kubischik M, Hoff-mann K, Zilles K, Fink GR. 2001. Polymodal motion processing in posterior parietal and premotor cortex: a human fMRI study strongly implies equivalencies between humans and monkeys. *Neuron*. 29:287–296.

Bruce C, Desimone R, Gross CG. 1981. Visual properties of neu-rons in a polysensory area in superior temporal sulcus of the macaque. *J Neurophysiol*. 46:369–384.

Cardin V, Smith AT. 2010. Sensitivity of human visual and vestibular cortical regions to egomotion-compatible visual stimulation. *Cereb Cortex*. 20:1964–1973.

Chapin JK, Woodward DJ. 1982. Somatic sensory transmission to the cortex during movement: phasic modulation over the locomotor step cycle. *Exp Neurol*. 78:670–684.

Chen A, DeAngelis GC, Angelaki DE. 2011a. Representation of vestibular and visual cues to self-motion in ventral intrapari-etal cortex. *J Neurosci*. 31:12036–12052.

Chen A, de Angelis GC, Angelaki DE. 2011b. Convergence of vestibular and visual self-motion signals in an area of the posterior sylvian fissure. *J Neurosci*. 31:11617–11627.

Colby CL, Duhamel JR, Goldberg ME. 1993. Ventral intraparietal area of the macaque: anatomic location and visual response properties. *J Neurophysiol*. 69:902–914.

Colin G. 2005. Chapter 1 - The taxonomy of primates in the laboratory context. In: Sonia W-C, BT-TLP, editors. *Handbook of Experimental Animals*. London: Academic Press, pp. 3–15.

Cottereau BR, Smith AT, Rima S, Fize D, Héjja-Brichard Y, Renaud L, Lejards C, Vayssière N, Trotter Y, Durand JB. 2017. Pro-cessing of Egomotion-consistent optic flow in the rhesus macaque cortex. *Cereb Cortex*. 27:330–343.

Delhaye BP, Long KH, Bensmaia SJ. 2018. Neural basis of touch and proprioception in primate cortex. *Compr Physiol*. 8:1575–1602.

Duffy CJ. 1998. MST neurons respond to optic how and transla-tional movement. *J Neurophysiol*. 80:1816–1827.

Dukelow SP, DeSouza JFX, Culham JC, van den Berg AV, Menon RS, Vilis T. 2001. Distinguishing subregions of the human MT+ complex using visual fields and pursuit eye move-ments. *J Neurophysiol*. 86:1991–2000.

Fan RH, Liu S, Deangelis GC, Angelaki DE. 2015. Heading tuning in macaque area v6. *J Neurosci*. 35:16303–16314.

Favorov OV, Nilaweera WU, Miasnikov AA, Beloozerova IN. 2015. Activity of somatosensory-responsive neurons in high subdivisions of SI cortex during locomotion. *J Neurosci*. 35:7763–7776.

Felleman DJ, Burkhalter A, Van Essen DC. 1997. Cortical connec-tions of areas V3 and VP of macaque monkey extrastriate visual cortex. *J Comp Neurol*. 379:21–47.

Fischer E, Bülthoff HH, Logothetis NK, Bartels A. 2012. Visual motion responses in the posterior cingulate sulcus: a com-parison to V5/MT and MST. *Cereb Cortex*. 22:865–876.

Fitzsimmons NA, Lebedev MA, Peikon ID, Nicolelis MAL. 2009. Extracting kinematic parameters for monkey bipedal walking from cortical neuronal ensemble activity. *Front Integr Neurosci*. 3:3.

Frank SM, Baumann O, Mattingley JB, Greenlee MW. 2014. Vestibular and visual responses in human posterior insular cortex. *J Neurophysiol*. 112:2481–2491.

Furlan M, Smith AT. 2016. Global motion processing in human visual cortical areas V2 and V3. *J Neurosci*. 36:7314–7324.

Galletti C, Gamberini M, Kutz DF, Fattori P, Luppino G, Matelli M. 2001. The cortical connections of area V6: an occipito-parietal network processing visual information. *Eur J Neurosci*. 13:1572–1588.

Gattass R, Sousa APB, Mishkin M, Ungerleider LG. 1997. Cortical projections of area V2 in the macaque. *Cereb Cortex*. 7:110–129.

Gibson JJ. 1950. *The Perception of the Visual World*. Boston: Houghton Mifflin.

Gu Y, Angelaki DE, DeAngelis GC. 2008. Neural correlates of multisensory cue integration in macaque MSTd. *Nat Neurosci*. 11:1201–1210.

Gu Y, Cheng Z, Yang L, Deangelis GC, Angelaki DE. 2016. Multisensory convergence of visual and vestibular heading cues in the pursuit area of the frontal eye field. *Cereb Cortex*. 26:3785–3801.

Guldin WO, Grüsser OJ. 1998. Is there a vestibular cortex? *Trends Neurosci*. 21:254–259.

Héjja-Brichard Y, Rima S, Rapha E, Durand J-B, Cottereau BR. 2020. Stereomotion processing in the nonhuman primate brain. *Cereb Cortex*. 30(8):4528–4543.

Hikosaka K, Iwai E, Saito HA, Tanaka K. 1988. Polysensory properties of neurons in the anterior bank of the caudal superior temporal sulcus of the macaque monkey. *J Neurophysiol*. 60:1615–1637.

Jenkinson M, Bannister P, Brady M, Smith S. 2002. Improved optimization for the robust and accurate linear registration and motion correction of brain images. *Neuroimage*. 17:825–841.

Jenkinson M, Beckmann CF, Behrens TEJ, Woolrich MW, Smith SM. 2012. Review FSL. *Neuroimage*. 62:782–790.

Jia X-Z, Wang J, Sun H-Y, Zhang H, Liao W, Wang Z, Yan C-G, Song X-W, Zang Y-F. 2019. RESTplus: an improved toolkit for resting-state functional magnetic resonance imaging data processing. *Sci Bull*. 64:953–954.

Karadimas SK, Satkunendrarajah K, Laliberte AM, Ringuette D, Weisspapir I, Li L, Gosgnach S, Fehlings MG. 2020. Sensory cortical control of movement. *Nat Neurosci*. 23:75–84.

Kimura T. 1992. Hindlimb dominance during primate high-speed locomotion. *Primates*. 33:465–476.

Koch MA, Norris DG, Hund-Georgiadis M. 2002. An investigation of functional and anatomical connectivity using magnetic resonance imaging. *Neuroimage*. 16:241–250.

Kravitz DJ, Saleem KS, Baker CI, Mishkin M. 2011. A new neural framework for visuospatial processing. *Nat Rev Neurosci*. 12:217–230.

la Fougère C, Zwergal A, Rominger A, Förster S, Fesl G, Dieterich M, Brandt T, Strupp M, Bartenstein P, Jahn K. 2010. Real versus imagined locomotion: a [18F]-FDG PET-fMRI comparison. *Neuroimage*. 50:1589–1598.

Leichnetz GR. 2001. Connections of the medial posterior parietal cortex (area 7m) in the monkey. *Anat Rec*. 263:215–236.

Loh KK, Hadj-Bouziane F, Petrides M, Procyk E, Amiez C. 2018. Rostro-caudal organization of connectivity between cingulate motor areas and lateral frontal regions. *Front Neurosci*. 11:753.

Luppino G, Matelli M, Camarda RM, Gallese V, Rizzolatti G. 1991. Multiple representations of body movements in mesial area 6 and the adjacent cingulate cortex: an intracortical microstimulation study in the macaque monkey. *J Comp Neurol*. 311:463–482.

Markov NT, Ercsey-Ravasz MM, Ribeiro Gomes AR, Lamy C, Magrou L, Vezoli J, Misery P, Falchier A, Quilodran R, Gariel MA *et al*. 2014. A weighted and directed interareal connectivity matrix for macaque cerebral cortex. *Cereb Cortex*. 24:17–36.

Markov NT, Misery P, Falchier A, Lamy C, Vezoli J, Quilodran R, Gariel MA, Giroud P, Ercsey-Ravasz M, Pilaz LJ *et al*. 2011. Weight consistency specifies regularities of macaque cortical networks. *Cereb Cortex*. 21:1254–1272.

Matelli M, Luppino G, Rizzolatti G. 1991. Architecture of superior and mesial area 6 and the adjacent cingulate cortex in the macaque monkey. *J Comp Neurol*. 311:445–462.

McLaren DG, Kosmatka KJ, Kastman EK, Bendlin BB, Johnson SC. 2010. Rhesus macaque brain morphometry: a methodological comparison of voxel-wise approaches. *Methods*. 50: 157–165.

McLaren DG, Kosmatka KJ, Oakes TR, Kroenke CD, Kohama SG, Matochik JA, Ingram DK, Johnson SC. 2009. A population-average MRI-based atlas collection of the rhesus macaque. *Neuroimage*. 45:52–59.

Passarelli L, Rosa MGP, Bakola S, Gamberini M, Worthy KH, Fattori P, Galletti C. 2018. Uniformity and diversity of cortical projections to precuneate areas in the macaque monkey: what defines area PGm? *Cereb Cortex*. 28:1700–1717.

Passarelli L, Rosa MGP, Gamberini M, Bakola S, Burman KJ, Fattori P, Galletti C. 2011. Cortical connections of area V6Av in the macaque: a visual-input node to the eye/hand coordination system. *J Neurosci*. 31:1790–1801.

Paxinos G, Huang XF, Toga AW. 2000. *The Rhesus Monkey Brain in Stereotaxic Coordinates*. San Diego, CA: Academic Press.

Picard N, Strick PL. 1996. Motor areas of the Medial Wall: a review of their location and functional activation. *Cereb Cortex*. 6(3):342–353.

Rizzolatti G, Luppino G. 2001. The cortical motor system. *Neuron*. 31:889–901.

Roos C, Zinner D. 2015. Diversity and evolutionary history of macaques with special focus on *Macaca mulatta* and *Macaca fascicularis*. In: Blümel J, Korte S, Schenck E, Weinbauer G, ediitors. *The Nonhuman Primate in Nonclinical Drug Development and Safety Assessment*. Amsterdam, The Netherlands: Elsevier, pp. 3–16.

Saleem K, Logothetis N. 2007. *A Combined MRI and Histology Atlas of the Rhesus Monkey Brain in Stereotaxic Coordinates*. Amsterdam, Boston: Elsevier/Academic Press.

Schlack A, Hoffmann K-P, Bremmer F. 2002. Interaction of linear vestibular and visual stimulation in the macaque ventral intraparietal area (VIP). *Eur J Neurosci*. 16:1877–1886.

Schmidt M. 2011. Locomotion and postural behaviour. *Adv Sci Res*. 5:23–39.

Serra C, Galletti C, Di Marco S, Fattori P, Galati G, Sulpizio V, Pitzalis S. 2019. Egomotion-related visual areas respond to active leg movements. *Hum Brain Mapp*. 40:3174–3191.

Sherrill KR, Chrastil ER, Ross RS, Erdem UM, Hasselmo ME, Stern CE. 2015. Functional connections between optic flow areas and navigationally responsive brain regions during goal-directed navigation. *Neuroimage*. 118:386–396.

Shipp S, Blanton M, Zeki S. 1998. A visuo-somatomotor pathway through superior parietal cortex in the macaque monkey: cortical connections of areas V6 and V6A. *Eur J Neurosci*. 10:3171–3193.

Smith AT, Beer AL, Furlan M, Mars RB. 2018. Connectivity of the cingulate sulcus visual area (CSv) in the human cerebral cortex. *Cereb Cortex*. 28:713–725.

Smith AT, Greenlee MW, DeAngelis GC, Angelaki DE. 2017. Distributed visual-vestibular processing in the cerebral cortex of man and macaque. *Multisens Res*. 30:91–120.

Smith AT, Wall MB, Thilo KV. 2012. Vestibular inputs to human motion-sensitive visual cortex. *Cereb Cortex*. 22:1068–1077.

Stern JT, Oxnard CE. 1973. Primate locomotion: some links with evolution and morphology. In: Hofer H Schultz AH Starck D, editors. *Primatologia*, Vol 4. Basel: Karger, pp. 723–886.

Takakusaki K. 2017. Functional Neuroanatomy for posture and gait control. *J Mov Disord*. 10:1–17.

Van Essen DC. 2002. Surface-based atlases of cerebellar cortex in the human, macaque, and mouse. *Ann N Y Acad Sci*. 978:468–479.

Van Essen DC, Drury HA, Dickson J, Harwell J, Hanlon D, Anderson CH. 2001. An integrated software suite for surface-based analyses of cerebral cortex. *J Am Med Inform Assoc*. 8: 443–459.

Vincent JL, Patel GH, Fox MD, Snyder AZ, Baker JT, Van Essen DC, Zempel JM, Snyder LH, Corbetta M, Raichle ME. 2007. Intrinsic functional architecture in the anaesthetized monkey brain. *Nature*. 447:83–86.

Vogt BA, Finch DM, Olson CR. 1992. Functional heterogeneity in cingulate cortex: the anterior executive and posterior evaluative regions. *Cereb Cortex*. 2:435–443.

Vogt BA, Pandya DN, Rosene DL. 1987. Cingulate cortex of the rhesus monkey: I. Cytoarchitecture and thalamic afferents. *J Comp Neurol*. 262:256–270.

Wall MB, Smith AT. 2008. The representation of Egomotion in the human brain. *Curr Biol*. 18:191–194.

Warren J, Kay BA, Zosh WD, Duchon AP, Sahuc S. 2001. Optic flow is used to control human walking. *Nat Neurosci*. 4:213–216.

Wirth AM, Frank SM, Greenlee MW, Beer AL. 2018. White matter connectivity of the visual-vestibular cortex examined by diffusion-weighted imaging. *Brain Connect*. 8:235–244.

Zhang D, Gao Z, Liang B, Li J, Cai Y, Wang Z, Gao M, Jiao B, Huang R, Liu M. 2019. Eyes closed elevates brain intrinsic activity of sensory dominance networks: a classifier discrimination analysis. *Brain Connect*. 9:221–230.